

1 A high-Arctic inner shelf–fjord system from the Last Glacial
2 Maximum to the Present: Bessel Fjord and SW Dove Bugt, NE
3 Greenland

4 Authors: Kevin Zoller¹; Jan Sverre Laberg¹; Tom Arne Rydningen¹, Katrine Husum² & Matthias
5 Forwick¹

6 ¹Department of Geosciences, UiT The Arctic University of Norway, Box 6050 Langnes, NO-
7 9037 Tromsø, Norway ²Norwegian Polar Institute, Box 6606 Langnes, NO-9296 Tromsø,
8 Norway

9 *Correspondence to:* Kevin Zoller (kevin.zoller3@gmail.com)

10 **Abstract**

11 The Greenland Ice Sheet (GrIS) responds rapidly to the present climate, therefore, its response
12 to the predicted future warming is of concern. To learn more about the impact of future climatic
13 warming on the ice sheet, decoding its behavior during past periods of warmer than present
14 climate is important. However, due to the scarcity of marine studies reconstructing ice sheet
15 conditions on the Northeast Greenland shelf and adjacent fjords, the timing of the deglaciation
16 over marine regions and its connection to forcing factors remain poorly constrained. This
17 includes data collected in fjords that encompass the Holocene Thermal Maximum (HTM), a
18 period in which the climate was warmer than it is at present. This paper aims to use new
19 bathymetric data and the analysis of sediment gravity cores to enhance our understanding of ice
20 dynamics of the GrIS in a fjord and inner shelf environment as well as give insight into the timing
21 of deglaciation and provide a palaeoenvironmental reconstruction of southwestern Dove Bugt
22 and Bessel Fjord since the Last Glacial Maximum (LGM). North-south oriented glacial
23 lineations, and the absence of pronounced moraines in southwest Dove Bugt, an inner
24 continental shelf embayment (trough), suggests the southwards and offshore flow of
25 Storstrømmen, the southern branch of the Northeast Greenland Ice Stream (NEGIS).
26 Sedimentological data suggests that an ice body, theorized to be the NEGIS, may have
27 retreated from the region slightly before ~11.4 cal. ka BP. The seabed morphology of Bessel
28 Fjord, a fjord terminating in southern Dove Bugt, includes numerous basins, separated by
29 thresholds. The position of basin thresholds, which include some recessional moraines, suggest
30 that the GrIS had undergone multiple halts or readvances during deglaciation, likely during one
31 of the cold events identified in the Greenland Summit temperature records. A minimum age of
32 7.1 cal. ka BP is proposed for the retreat of ice through the fjord to or west of its present-day
33 position in the Bessel Fjord catchment area. This suggests that the GrIS retreated from the
34 marine realm in early Holocene, around the onset of the HTM in this region, a period when the
35 mean July temperature was at least 2-3 °C higher than at present and remained at or west of
36 this onshore position for the remainder of the Holocene. The transition from predominantly mud
37 to muddy sand layers in a mid-fjord core at ~4 cal. ka BP may be the result of increased
38 sediment input from nearby and growing ice caps. This shift may suggest that in the Late
39 Holocene (Meghalayan), a period characterized by a temperature drop to modern values, ice
40 caps in Bessel Fjord probably fluctuated with greater sensitivity to climatic conditions than the
41 NE sector of the GrIS.

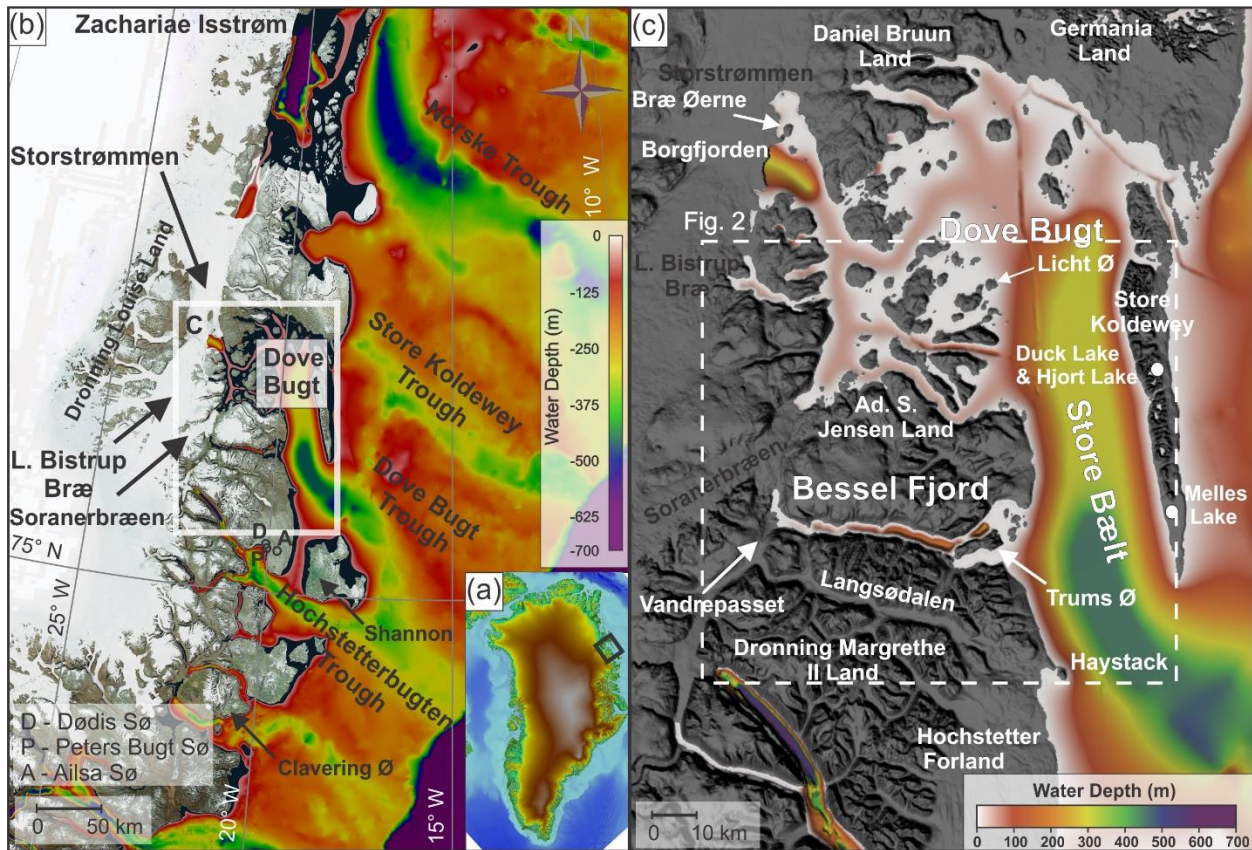
42 1. Introduction

43 Ice mass loss from the Greenland Ice Sheet (GrIS) has accelerated during the 21 century,
44 making it the largest individual contributor to sea level rise (King et al., 2020). This introduction
45 of a substantial quantity of fresh water may have ramifications for global ocean circulations as
46 well as the climate (Rahmstorf et al., 2015). Approximately 12% of the ice from the GrIS is
47 transported to the coast through the Northeast Greenland Ice Stream (NEGIS) (Khan et al.,
48 2014; Joughin et al., 2001) and therefore has a substantial impact on the mass balance of the
49 ice sheet and a potential to contribute to sea level rise. Currently, two of the three marine
50 terminating outlet glaciers that are supplied by the NEGIS are in retreat (Mouginot et al., 2015),
51 where the southernmost branch, Storstrømmen in Dove Bugt (Figs. 1a & 1b), is currently in a
52 building phase following a 1978-1984 surge (Khan et al., 2014; Reeh et al., 1994). While there
53 are numerous studies on the current state of the NEGIS during the past decades to century,
54 there is a scarcity of data concerning the position and dynamics of the ice stream, and other
55 local Northeast Greenland outlet glaciers, on a multi-century to millennia scale over marine
56 regions. Considering that the global mean temperature is expected to continue to rise (Stocker
57 et al., 2013), and that the Arctic will experience an amplification effect (Cohen et al., 2014),
58 looking to the past, especially during warmer than present periods (i.e., the Holocene Thermal
59 Maximum (HTM)), may provide an important insight into the future behavior of the ice sheet.

60 Marine studies have found evidence for past advancement and retreat of the GrIS and NEGIS
61 along the continental shelf offshore Northeast Greenland (Evans et al., 2009; Winkelmann et al.,
62 2010; Arndt et al., 2015, 2017; Laberg et al., 2017; Arndt, 2018; Olsen et al., 2020; Syring et al.,
63 2020; Davies et al., 2022; Hansen et al., 2022; Jackson et al., 2022). Geomorphological findings
64 in Store Koldewey Trough (~76°N), a major shelf trough northeast of the study area (Fig. 1b),
65 suggests that the ice sheet may have reached the shelf break in this area during the LGM (Last
66 Glacial Maximum) (Laberg et al., 2017; Olsen et al., 2020). However, further north (~79.4°N),
67 findings by Rasmussen et al. (2022) indicate that some regions near the shelf break were ice
68 free during the LGM despite Arndt et al. (2017) positioning the ice front at its maximum LGM
69 position at the outer shelf. A concise understanding of the timing and dynamics of the ice sheet
70 over the NE Greenland shelf during the subsequent deglaciation of the marine realm remains to
71 be established as very few dated cores have been recovered. Terrestrial dating (e.g.,
72 cosmogenic nuclide dates and lake studies) has provided further insight into when terrestrial
73 regions had become deglaciated, and how the climate has changed in these areas (e.g., Björck
74 and Persson, 1981; Björck et al., 1994; Wagner et al., 2008; Klug et al., 2009a; Schmidt et al.,
75 2011; Skov et al., 2020; Larsen et al., 2020). However, only recently has terrestrial data been
76 integrated with marine data to establish a detailed deglaciation chronology of the shelf, coastal
77 and fjord regions (Davies et al., 2022; Larsen et al., 2022).

78 Swath bathymetry and gravity cores data from southwestern Dove Bugt (i.e., Store Bælt) and
79 Bessel Fjord (Fig. 1), presented for the first time in this study, has been used to further refine
80 our understanding of how the GrIS responded to changes in palaeoclimatic conditions from the
81 LGM through the Holocene, including the HTM. Through this analysis we aim to reconstruct
82 regional ice dynamics from both full-glacial conditions and during overall retreat and put our
83 findings into the larger context of the dynamics of the Northeast Greenland Ice Sheet during
84 these periods. Additionally, this study aims to refine our understanding about the timing of
85 deglaciation over marine areas and compare findings to nearby terrestrial regions including the
86 Store Koldewey and Hochstetter Forland/Shannon Ø. Results will also contribute to our

87 understanding of palaeoenvironmental conditions throughout the Holocene for the NE
 88 Greenland fjords and inner shelf areas.



89
 90 *Figure 1. (a) An image of Greenland, using IBCAO 4.0 400x400m (Jakobsson et al., 2020), with a black box*
 91 *surrounding the study area. (b) Bathymetry of Northeast Greenland displayed using IBCAO 4.0 200x200m data*
 92 *(Jakobsson et al., 2020) and land is displayed using a World Imagery satellite image (Earthstar Geographics, Esri,*
 93 *HERE, Garmin, FAO, NOAA, USGS) made available through GlobalMapper. The white box surrounds the position of*
 94 *Fig. 1c. (c) Bathymetry of Dove Bugt and Bessel Fjord and surrounding land areas displayed using the IBCAO 4.0*
 95 *200x200m data (Jakobsson et al., 2020). Locations mentioned in the text are labelled here. The position of Fig. 2 is*
 96 *within the white dashed box.*

97 2. Regional Setting and Environmental History

98 Bessel Fjord is a west-east running fjord between Adolf S. Jensen Land and Dronning
 99 Margrethe II Land (Fig. 1c). The western end of the fjord contains the southern outlet glacier
 100 Soranerbræen, which also has a second outlet to the north in a tributary fjord to inner Dove Bugt
 101 (Fig. 2). Several ice caps are positioned across the length of the fjord (Figs. 2 & 3), some of
 102 which have several generations of moraines and glaciofluvial outlets that enter the fjord.
 103 Colluvial fans and rivers have been observed across the length of the fjord in satellite images
 104 and while surveying the fjord. Multiple islands are located at the entrance of Bessel Fjord, the
 105 largest of which, Trums Ø, splits the entrance into two main inlets (Figs. 1c & 2). From the
 106 termination of Soranerbræen to the entrance of the fjord measures ~60 km in length. The width
 107 of the fjord ranges from 1.8 to 3.7 km.

108 To the west of Bessel Fjord and Soranerbræen is the larger glacier L. Bistrup Bræ, which flows
 109 northwards and has an outlet in Borgfjorden, another tributary fjord to inner Dove Bugt (Fig 1).

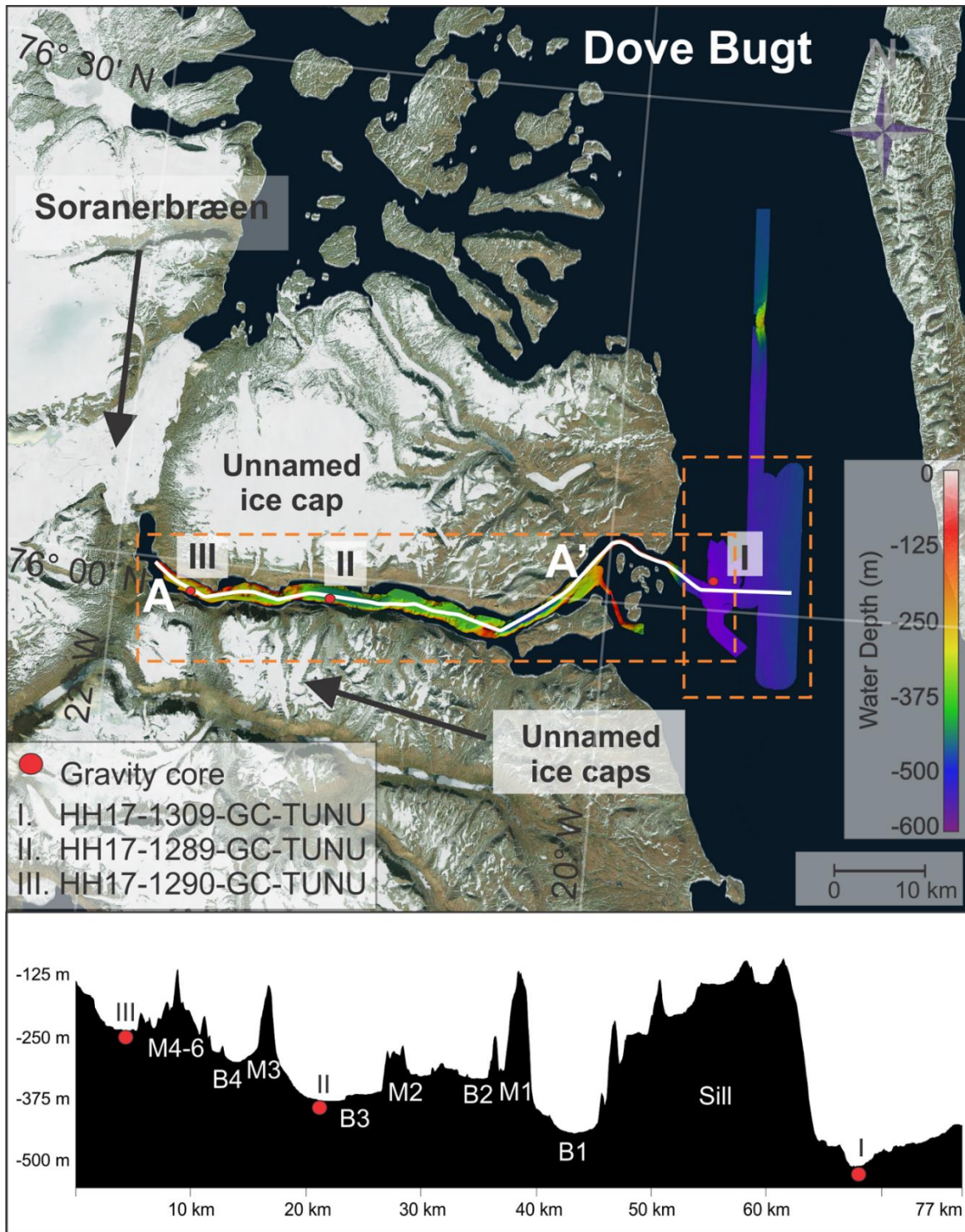
110 Here it is confluent with the southward flowing NEGIS outlet glacier, Storstrømmen (Rignot et
111 al., 2022). Studies of modern Soranerbræen, L. Bistrup Bræ and Storstrømmen suggest that
112 they all have separate drainage basins (Krieger et al., 2020). Storstrømmen and L. Bistrup Bræ
113 are two of the largest surge-type glaciers in the world (Higgins, 1991) with a surge periodicity of
114 approximately 70 years (Mouginot et al., 2018).

115 Bathymetry of inner Dove Bugt and tributary fjords has revealed that there are no natural large
116 passageways for the warm, salty, subsurface Atlantic Intermediate Water to impact these
117 glaciers at present, therefore it has been suggested that ocean waters do not play a large role in
118 the evolution of Storstrømmen, L. Bistrup Bræ and the northern outlet of Soranerbræen, and
119 that their grounding line retreat is mostly caused by ice thinning (Rignot et al., 2022).

120 Mega-scale glacial lineations (MSGSL) identified in Store Koldewey Trough on the continental
121 shelf have been interpreted as evidence for the expanse of this sector of the GrIS to the shelf
122 break during the LGM (Laberg et al., 2017; Olsen et al., 2020). This is further supported by the
123 presence of recessional moraines and grounding zone wedges, which suggests a complex
124 deglaciation of this part of the shelf area (Arndt et al., 2015, 2017; Laberg et al., 2017; Arndt,
125 2018; Olsen et al., 2020). Olsen et al. (2020) has suggested that deglaciation in the Store
126 Koldewey Trough may have occurred in two stages: first, an initial retreat as a result of eustatic
127 sea level rise caused by melting ice at lower latitudes (Lambeck et al., 2014), followed by a
128 melting phase driven by ocean warming. So far, the timing of the onset of the deglaciation is not
129 known. Across the GrIS, deglaciation is believed to be asynchronous, with factors such as
130 topography and local ice dynamics playing a large role with ice retreat in conjunction with
131 climate change (Bennike & Björck, 2002; Funder et al., 2011; Ó Cofaigh et al., 2013; Hogan et
132 al., 2016).

133 A recent study by Jackson et al. (2022) of the inner shelf east of the Clavering Ø (~74°N; Fig.
134 1b) indicated that during the late Younger Dryas, this sector of the GrIS had reached a more
135 landward position, in conformity with Funder et al. (2021). During this period, the inner shelf
136 bottom water was characterized by anomalously high temperatures, interpreted to have played
137 a role in the ice retreat and leading to the termination of the Younger Dryas stadial. This was
138 followed by the onset of the East Greenland Current, as seen from cooler bottom water from the
139 Early Holocene on (Jackson et al., 2022).

140 Further north, east of marine terminating glacier Zachariae Isstrøm (~78° 30N; Fig. 1b), the
141 deglaciation of the NEGIS from the inner shelf was found to have occurred as early as 12.5 cal.
142 ka BP, likely before 13.4 cal. ka BP (Davies et al., 2022). Here, inflow of warmer water (Atlantic
143 Water) may have played a role. This part of the shelf was covered by an ice shelf from 13.4 to
144 11.2 cal. ka BP (including the Younger Dryas), retreating and leading to open water conditions
145 from the earliest Holocene; 11.2-10.8 cal. ka BP, before readvancing from 10.8 to 9.6 cal. ka
146 BP, finally retreating from 9.6 to 7.9 cal. ka BP. At 7.9 cal. ka BP there was a drastic shift in
147 ocean circulation at this site with a sharp decline in Atlantic Water corresponding to an increase
148 in Polar Water influx (Davies et al., 2022). Pados-Dibattista et al. (2022), studying another core
149 from the NE Greenland shelf (more seaward, in a mid-shelf position north of the Norske Trough
150 at ~79°N), found that during the early Holocene (9.4 to 8.2 cal. ka BP), the East Greenland
151 Current was highly stratified with cold surface water overlying warm Atlantic subsurface water.



152

153 *Figure 2. Study area with the bathymetric data showing the locations of the sediment cores presented in this study.*
 154 *The lower panel is a profile along the length of Bessel Fjord, A-A'. Sediment cores are labelled I, II and III. Satellite*
 155 *image is displayed using a World Imagery satellite image (Earthstar Geographics, Esri, HERE, Garmin, FAO, NOAA,*
 156 *USGS) made available through GlobalMapper.*

157



158

159 *Figure 3. Image of an ice lobe from an ice cap near gravity core HH17-1289-GC-TUNU. Two sets of coarse-grained*
160 *terminal morainal ridges are indicated by number and arrow. See Fig. 6b for the position of the modern ice lobe. The*
161 *photograph was taken by Torger Grytå on a 2017 TUNU cruise.*

162 Following the 8.2 ka event, the interval from 8.2 to 6.2 cal. ka BP was followed by the warmest
163 Holocene bottom water conditions on the shelf. Afterwards, conditions returned to those seen
164 prior to 8.2 cal. ka BP due to increased Polar Water transport strengthening the East Greenland
165 Current (Pados-Dibattista et al., 2022).

166 Terrestrial studies of Dronnings Margrethe II Land, Germania Land and adjacent areas have
167 identified a complex assortment of moraines that are believed to have formed during the Kap
168 Mackenzie, Muschelbjerg, Nanok I and Nanok II stadials (Hjort, 1979, 1981; Hjort and Björck,
169 1983; Björck et al., 1994; Landvik, 1994). The exact ages of these stadials remain unclear
170 (Table 1), yet Larsen et al. (2022) suggests that Nanok-stadial moraines found in Store
171 Koldewey formed synchronously with the Milne Land moraines of Scoresby Sund which date to
172 the Allerød to early Younger Dryas and Preboreal time (Kelly et al., 2008; Levy et al., 2016).

173 The position of striations on Store Koldewey and lateral moraines on coastal slopes between
174 Bessel Fjord and Haystack have been interpreted as evidence for ice flowing out of Dove Bugt
175 and Bessel Fjord during the Muschelbjerg stadial, southwards through Store Bælt and turning
176 eastwards around the southernmost mountains of Store Koldewey (Hjort, 1981). Early studies of
177 the region noted glacial and glaciofluvial deposits (e.g., moraine plateau, terminal moraines,
178 eskers and sandurs) on Hochstetter Forland that are believed to have formed during this period
179 (Hjort, 1979, 1981).

180 Table 1. Previously published stadial information for the Dove Bugt region as well as age estimates used in this
 181 study.

Stadials	Studies					Age estimate used in this study
	<i>Hjort & Björck (1983)</i>	<i>Funder et al., (1998)</i>	<i>Kelly et al. (2008)</i>	<i>Vasskog et al. (2015)</i>	<i>Larsen et al. (2022)</i>	
<i>Nanok II</i>	10.1-9.5 cal. ka BP	Preboreal (ending at ca. 9.7 cal. ka BP)	Younger Dryas and Early Holocene (13-11.6 ka (G-III), 11.7-10.6 ka (G-II))	Close to Bølling– Allerød transition, and late Younger Dryas (~14 cal. ka BP (G III), ~12 cal. ka BP (G-II))	Preboreal	Preboreal
<i>Nanok I</i>	Older than 14 cal. ka BP, possibly between 15 and 19 cal. ka BP	~48 cal. ka BP (Hjort, unpublished data)			Late Allerød to early Younger Dryas	Late Allerød to early Younger Dryas
<i>Nanok 0</i>						?
<i>Muschelbjerg</i>	Saalian (or older)?					Saalian (or older)?
<i>Kap Mackenzie</i>	Saalian (or older)?					Saalian (or older)?

182
 183 Lateral moraines and glacial striations oriented along the axis of Langsodal (also referred to as
 184 Langsødal; Fig. 1c), a nearby valley south of and sub-parallel to Bessel Fjord, have been
 185 interpreted as evidence for glacial confinement within the valley during an undifferentiated
 186 Nanok stadial (Hjort 1979; Hjort, 1981). This differs from striations that have also been identified
 187 in the valley along more weathered surfaces that are oriented in a southwestern direction (Hjort,
 188 1979).

189 The outer coastal regions of North and Northeast Greenland are believed to have been
 190 deglaciated between 12.8 and 9.7 ka BP and present ice positions were reached between 10.8
 191 to 5.8 ka BP (Larsen et al., 2022). Cosmogenic nuclide dates from Store Koldewey, first
 192 collected by Håkansson et al. (2007), and later Skov et al. (2020) and Larsen et al. (2022),
 193 suggest that ice retreated from the continental shelf and reached the upper and lower sections
 194 of the island by 12.3 and 12.7 ka BP, respectively. In contrast, Biette et al. (2020) found
 195 evidence of the deglaciation of Clavering Ø at 16.2 ka BP, with readvances at 11.3, 10.8, 3.3,
 196 1.2 and 0.37 ka BP. Additional cosmogenic nuclide findings indicate that Trums Ø, in outer

197 Bessel Fjord, may have become deglaciated around 12.6 ka BP and Vandrepasset, onshore
198 inner Bessel Fjord by 8.6 ka BP (Larsen et al., 2022).

199 Findings from macrofossil remains (Bennike & Björck, 2002) and lacustrine sedimentary records
200 (Cremer et al., 2008) suggest that coastal regions were deglaciated in a ~1500 year span after
201 the start of the Holocene (Klug et al., 2016). To the north of Store Koldewey, a minimum date
202 for deglaciation in Germania Land of 9.5 cal. ka BP has been proposed (Landvik, 1994),
203 whereas to the south in southern Dronning Margrethe II Land, a minimum date of 11.2 cal. ka
204 BP has been suggested (Bennike & Weidick, 2001). Lake studies on aquatic organisms at
205 Björck Lake and Hjort Lake on Store Koldewey (Fig. 1c) indicate that the island was at its
206 warmest between ~8 and 4 cal. ka BP, (Wagner et al., 2008; Klug et al., 2009; Schmidt et al.,
207 2011), although findings from Melles Lake (Fig. 1c) suggest that the earliest onset of warmth
208 during the Holocene may have occurred at ~ 10 cal. ka BP (Klug et al., 2009; Briner et al.,
209 2016). On Hochstetter Forland (Fig. 1c), pollen assemblages from Dødis Sø, Peters Bugt Sø
210 and Ailsa Sø suggest that the temperatures were at their highest between 8.8 and 5.6 cal. ka
211 BP (Björck & Persson, 1981; Björck et al., 1994). These findings indicate that the HTM was not
212 uniform across East Greenland, as also described by Briner et al. (2016).

213 To the south, offshore the Kejser Franz Josef Fjord system (~73°N), a detailed biomarker record
214 finds this part of the shelf dominated by seasonal sea ice throughout the Late Holocene (<~5
215 cal. ka BP) and extended concentrations from 5.2 to 2.2 and 1.3 cal. ka BP to present. Short-
216 term variability was also seen for this area for the last 2.2 cal. ka BP, corresponding to the
217 climatic events of this period (Kolling et al., 2017).

218 **3. Material and Methods**

219 Swath bathymetry and three sediment cores were collected in southwestern Dove Bugt and
220 Bessel Fjord during an expedition aboard RV *Helmer Hanssen* of UiT The Arctic University of
221 Norway in September 2017, being part of the TUNU program (Fig. 2; Christiansen, 2012). The
222 swath bathymetry data was obtained using a Kongsberg Maritime Simrad EM 302 multibeam
223 echo sounder. It was gridded using Petrel software, and geomorphological interpretations were
224 made using Global Mapper 18. Surfaces were developed using a 5x5m grid cell size while a
225 surface created from an International Bathymetric Chart of the Arctic Ocean (IBCAO) dataset
226 4.0 with a 200x200m grid cell size (Jakobsson et al., 2020).

227 Two soft sediment gravity cores were retrieved from Bessel Fjord (HH17-1289-GC-TUNU &
228 HH17-1290-GC-TUNU) and one southwest of Dove Bugt in the sound Store Bælt (HH17-1309-
229 GC-TUNU) (Fig. 2 & Table 2). Prior to splitting the cores, physical properties were measured
230 using a GEOTEK Multi Sensor Core Logger (MSCL-S). The cores were placed in the laboratory
231 for 24 hours prior to obtaining physical measurements to ensure that each core temperature
232 reached equilibrium with the laboratory to avoid distorting p-wave values (Weber et al., 1997).

233 A GEOTEK MSCL X-ray Computed Tomographic imaging machine was also used to scan the
234 unopened core sections to create X-ray radiographic images. After each core was split and
235 cleaned, the characteristics of the sedimentary surface were logged (i.e., structures,
236 bioturbation, grain size, lithological boundaries, etc.), sediment color was noted using the
237 Munsell Soil Color Chart and lithofacies were assigned based on Eyles et al. (1983)
238 classification system. Colored images of the core sections were then obtained using an
239 Avaatech XRF core scanner.

240 *Table 2. Information on the position, water depth and recovery length of each gravity core. Note that the core names*
 241 *are abbreviated in the text.*

Location	Inner Bessel Fjord	Mid-Bessel Fjord	Southeastern Dove Bugt
Coring station	HH17-1290	HH17-1289	HH17-1309
Latitude [N]	75° 58' 34.5907"	75° 58' 11.4928"	76° 01' 34.0387"
Longitude [W]	21° 07' 13.1055"	21° 41' 48.0278"	19° 34' 31.3190"
Water depth [m]	372	225	512
Recovery [cm]	534.5	245.5	474.55

242

243 Molluscs and benthic foraminifera were recovered from each core for the purpose of
 244 radiocarbon dating of lithofacies boundaries. This was, however, not always possible due to the
 245 low content of foraminifera and molluscs in these cores which also restricted the number of
 246 dates that could be obtained. Two adjacent 1 cm thick sediment slices were successfully
 247 sampled from select positions across cores HH17-1290 and HH17-1309. Samples were then
 248 wet sieved at 1 mm, 100 µm and 63 µm meshes, respectively. Benthic foraminifera from the
 249 100-µm size fraction were extracted for radiocarbon dating. Radiocarbon dating was carried out
 250 at the MICADAS radiocarbon laboratory at Alfred Wegener Institute, Helmholtz Centre for Polar
 251 and Marine Research, Germany. The radiocarbon dates were calibrated using the online
 252 version of OxCal 4.4 (<https://c14.arch.ox.ac.uk/oxcal.html#program>) and the Marine20
 253 calibration curve (Heaton et al., 2020), as the calibrated ¹⁴C samples are younger than 11.5 cal.
 254 ka BP (Heaton et al., 2022). We are using a ΔR of -10 ± 60 in conformity with Jackson et al.
 255 (2022). Previously reported radiocarbon dates from this area that are relevant to our study have
 256 been recalibrated using Marine20 for marine samples under 11.5 cal. ka BP and IntCal20 for
 257 terrestrial samples (Reimer et al., 2020). One marine sample older than 11.5 cal. ka BP has
 258 also been included (Table 3). In the Arctic, including our study area, calibration of marine
 259 samples by Marine20 is not recommended for samples older than 11.5 cal. ka BP (see Heaton
 260 et al. (2022)), therefore, this calibrated age is treated with caution.

261 A Beckman Coulter LS 13 320 Multi-Wavelength Laser Diffraction Particle Size Analyzer was
 262 used to perform sediment grain size analysis. Sediment was sampled in mostly 10 cm intervals
 263 across HH17-1309, where samples taken from the other two cores were selected from specific
 264 positions. Samples were treated in HCl and H₂O₂ and a pre-heated VWB 18 Thermal Bath.
 265 Samples were then cleaned using distilled water, placed through multiple runs through a
 266 centrifuge and heated in an oven to remove water content. Approximately 0.2 grams of
 267 sediment were then separated and placed in a container with 20 ml of water and moved to a
 268 shaking table for over 48 hours. A few drops of Calgon were added to each sample, which was
 269 then placed into a Branson 200 ultrasonic cleaner for ~7 minutes and shaken briefly before
 270 being poured through a >2 mm mesh and into the particle size analyzer. Grains between the
 271 size of 0.4 µm and 2000 µm were counted and underwent three separate runs. GRADISTAT
 272 Excel-software was used to calculate the mean of the three runs. Sediment names used in
 273 reference to this analysis are based on Folk (1954) and mean grain size from the methodology
 274 published by Folk & Ward (1957).

275

276

277 Table 3. Other published radiocarbon dates and their recalibrated ages using Marine20 (and an ΔR of -10 ± 60 in
 278 conformity with Jackson et al. (2022)) and IntCal20 for aquatic moss samples. *The age of sample Lu-1298 from
 279 Shannon is above what is recommended by Heaton et al., (2022) for use with Marine20. This date was considered an
 280 outlier and therefore not taken into consideration by the authors and Bennike and Björck (2002). Therefore, this date
 281 is also rejected in the present study.

Location	Material	Lab nr.	¹⁴ C age	¹⁴ C cal BP (1 σ range)	¹⁴ C cal BP (median)	Reference
Shannon	shell	Lu-1298*	19000 \pm 190	21855-22325	22078	Hjort, 1981; Hjort, 1979
Hochstetter F.	shell	Lu-1289	9190 \pm 90	9572-9926	9779	Hjort, 1981; Hjort, 1979
Shannon	shell	Lu-1389	9370 \pm 90	9865-10195	10015	Hjort, 1981; Hjort, 1979
Hochstetter F.	shell	Lu-1386	9400 \pm 90	9896-10220	10054	Hjort, 1981; Hjort, 1979
Hochstetter F.	shell	Lu-1300:1	9470 \pm 90	9970-10322	10157	Hjort, 1981; Hjort, 1979
Hochstetter F.	shell	Lu-1300:2	9520 \pm 90	10084-10412	10229	Hjort, 1981; Hjort, 1979
Hochstetter F.	shell	Lu-1384	9810 \pm 95	10409-10794	10617	Hjort, 1981; Hjort, 1979
Ardencaple Fjord	shell	Lu-1390	8570 \pm 85	8864-9200	9022	Hjort, 1981; Hjort, 1979
Kildedalen	shell	Lu-1303	8930 \pm 90	9290-9573	9447	Hjort, 1981; Hjort, 1979
Snenæs	Mya truncata,	T-9372	8265 \pm 95	8434-8768	8619	Landvik, 1994
	Hiatella arctica					
Hvalrosodden moraine	Nuculana	TUa-123	8685 \pm 95	9006-9315	9166	Landvik, 1994
	pernula					
Hvalrosodden moraine	Nuculana	TUa-124	9045 \pm 90	9438-9741	9596	Landvik, 1994
	pernula					
Hvalrosodden	Mya truncata	T-9361	8190 \pm 95	8360-8663	8523	Landvik, 1994
Hvalrosodden	Mya truncata,	T-9370	7930 \pm 120	8681-9085	8890	Landvik, 1994
	Hiatella arctica					
Hvalrosodden	Mya truncata	T-9371	7490 \pm 115	8186-8502	8348	Landvik, 1994
Peters Bugt	Portlandia	Ua-2787	10260 \pm 105	11071-11444	11253	Björck et al., 1994
	arctica					
Peters Bugt Sø	Hiatella arctica	Lu-3516	9640 \pm 90	10222-10527	10382	Björck et al., 1994
Storstrømmen Sound	Mya truncata &	K-6098	5180 \pm 95	5220-5520	5352	Weidick et al., 1994
	Hiatella arctica					
Storstrømmen Sound	Mya truncata	K-5494	4910 \pm 85	4865-5175	5028	Weidick et al., 1994
Storstrømmen Sound	Mya truncata	K-5493	4840 \pm 90	4793-5117	4943	Weidick et al., 1994
Storstrømmen Sound	Hiatella arctica	Ua-3347	5030 \pm 75	5023-5311	5166	Weidick et al., 1994
Storstrømmen Sound	Hiatella arctica	Ua-3350	4180 \pm 60	3944-4225	4082	Weidick et al., 1994
	Balanoptera					
Storstrømmen Sound	physalus	K-6096	3630 \pm 90	3230-3530	3380	Weidick et al., 1994
Storstrømmen Sound	Hiatella arctica	Ua-3349	3725 \pm 60	3371-3616	3496	Weidick et al., 1994
	Hiatella arctica					
Storstrømmen Sound	& Mya truncata	K-6097	3230 \pm 85	2749-3024	2897	Weidick et al., 1994
Storstrømmen Sound	Hiatella arctica	Ua-3348	1815 \pm 55	1115-1317	1217	Weidick et al., 1994
	Warnstorfia					
Hjort Lake	exannulata	Poz-6194	8260 \pm 50	8456-8722	8602	Wagner et al., 2008
Duck Lake	Aquatic moss	LuS-6525	8690 \pm 230	9527-10145	9775	Klug et al., 2009

282

283

284

285

286 4. Results

287 4.1. Seafloor landforms in SW Dove Bugt (Store Bælt)

288 4.1.1. Elongated Lineations - Glacial Lineations

289 Slightly curved sub-parallel lineations, oriented sub-parallel to the axis of Dove Bugt, are the
290 most pronounced landforms in this part of the study area. They are oriented N-NW in the south
291 and N-NE in the north (Fig. 4). The most frequently identified positive lineations (ridges) are 35-
292 50 m in width, <1-3 m in height and between 1 and 10 km in length. Length to width ratios are
293 frequently >10:1. At elevations shallower than 435 m depth, near the center of Store Bælt, the
294 lineations are wider (e.g., 60-150 m wide), and occasional merging and overlapping of lineations
295 occur (Fig. 4e). Wider lineations, often identified in the southern section of the study area (Fig.
296 4b), have also been identified with widths, lengths and heights ranging from 200-650 m, 3-8 km,
297 and 4.5-15 m, respectively. Length to width ratios here are 7:1 to >10:1. Some of the larger
298 lineations are superimposed by smaller lineations. Lateral ridges have also been identified in
299 clusters overprinting the lineations (Fig. 4c), where furrows have been found cross cutting
300 lineations (Fig. 4d). Lateral ridges measure 0.5 to 2 m in height and are approximately 45 to 250
301 m apart.

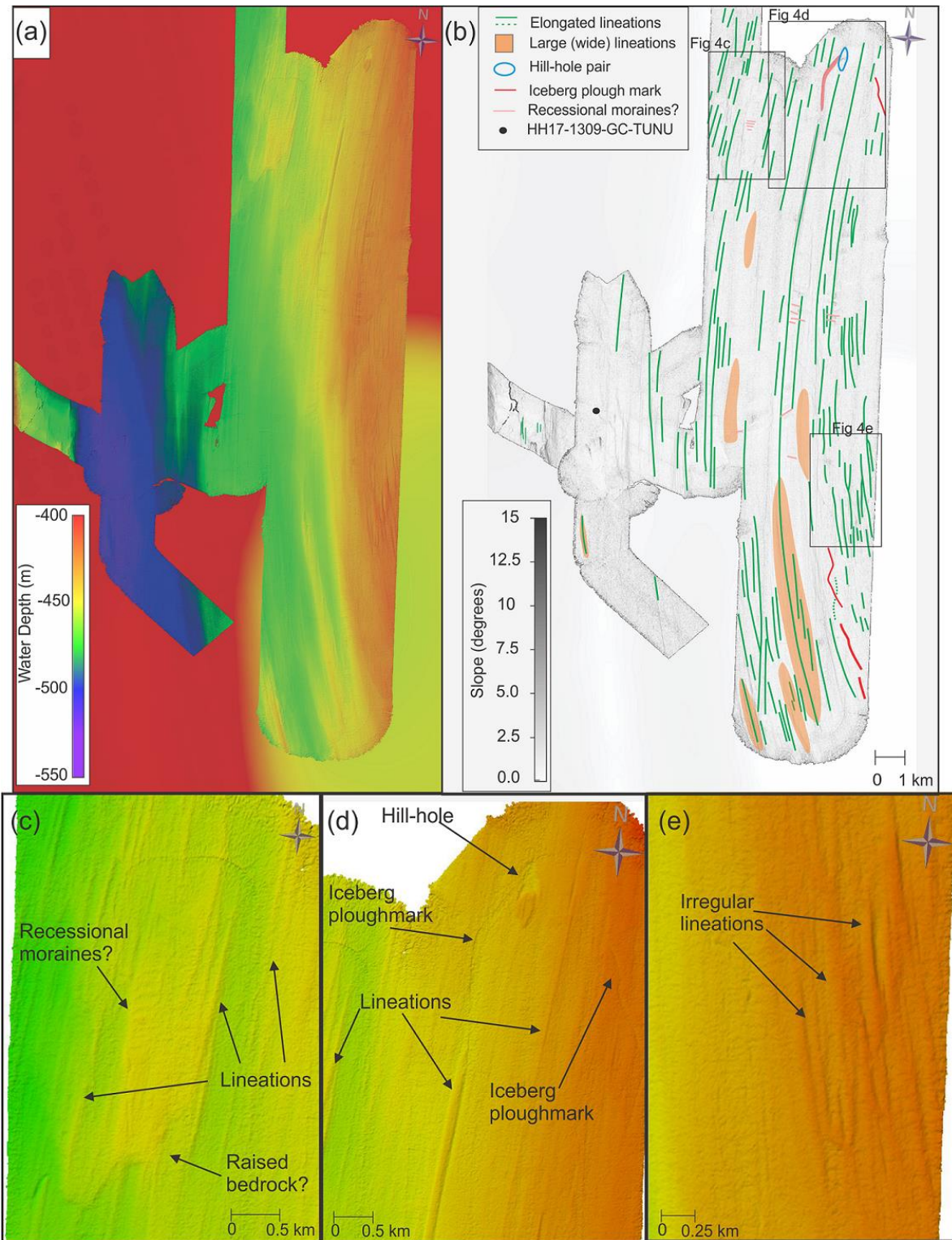
302 These elongated lineations are interpreted as glacial lineations (e.g., Ó Cofaigh, 2005). The
303 thinner, more common lineations (with length/width-ratios >10:1) have been interpreted as
304 mega-scale glacial lineations (MSGSL), and such landforms are commonly associated with
305 palaeo-ice stream environments (e.g., Stokes & Clark, 2001). Glacial lineations have been
306 identified in numerous continental shelf regions around Greenland (Evans et al., 2009;
307 Dowdeswell et al., 2014; Slabon et al., 2016; Laberg et al., 2017; Newton et al., 2017; Arndt,
308 2018; Batchelor et al., 2018; Jakobsson et al., 2018). While the mechanism behind the
309 formation of these features are still being debated, some authors have suggested that they may
310 have formed through meltwater flooding (Shaw et al., 2008), groove-ploughing (Clark et al.,
311 2003) or the transverse flow in basal ice (Schoof and Clarke, 2008). King et al. (2009) favored
312 aspects of the dilatant till instability model that could explain the development of MSGSLs on a
313 decadal timescale. Sets of ridges that overprint the glacial lineations have been interpreted as
314 recessional moraines, where furrows have been interpreted as iceberg plough marks.

315 4.1.2. Depression and Mound- Hill-Hole Pair

316 In northern Store Bælt, a 200 by 450 m wide, 3-4 m deep depression has been identified next to
317 a mound with a width and height of 235 by 450 m and 3-4 m, respectively (Fig. 4d). The
318 depression overprints N-S trending lineations, although the mound contains lineations on its
319 surface.

320 This depression and mound have been interpreted as a hill-hole pair. These landforms can form
321 when ice-thrust rafts of sediment are removed from the bed by cold-based, slow-flowing ice that
322 transports the sediment that was once in the depression (Hogan et al., 2010; Klages et al.,
323 2013, 2015). In this instance, a south bound ice stream may have removed frozen sedimentary
324 material and deposited it further south. This interpretation is in conformity with studies from
325 other high-latitude continental shelves where subglacial hill-hole pairs are interpreted as formed
326 by ice frozen to the seafloor bed (Sættem, 1990; Ottesen et al., 2005).

327



328

329 *Figure 4. Bathymetric maps from SW Dove Bugt. (a) Seafloor relative to water depth with IBCAO 4.0 displayed in the*
 330 *background (Jakobsson et al., 2020). (b) The main landforms and slope angles of the seafloor in SW Dove Bugt.*
 331 *Locations of Figs. 4c-e are indicated. (c) Bathymetry of the northwestern section of the study area. (d) Bathymetry of*
 332 *the northeaster part of the study area. (e) Bathymetry of the eastern part of the study area showing irregularly shaped*
 333 *glacial lineations.*

334 4.2. Sea floor landforms in Bessel Fjord

335 4.2.1. Large scale geomorphology

336 Bessel Fjord contains a variety of basins that are separated by different styles of sills (Figs. 2, 5
337 & 6). The outermost sill is at the fjord's entrance, and it commonly ranges in depth from 50 to
338 200 m, with major sections reaching above (and near) the water surface as there are islands in
339 the fjord entrance. Four large basins that are elongated in a west-east direction have been
340 identified in Bessel Fjord (B1-B4). The deepest basin, Basin 1 (B1), is the closest to the fjord
341 entrance and is separated from basin 2 (B2) by a >215 m high sill (M1) that is steeper to the
342 east (Figs. 2 & 5). Basin 3 progressively deepens westwards, with a maximum depth of 380 m.
343 A ~70 to 160 m asymmetrical sill (M3; Figs. 2 & 5) that is steeper on its east side separates
344 Basin 3 from basin 4. Basin 4 is the shallowest basin (~280-300 m) and is adjacent to multiple
345 smaller basins that are primarily at lower points of elevation. The fjord also contains smaller
346 basins that are raised relative to the average seafloor depth (Fig. 6e). Features interpreted as
347 bedrock mounds have also been identified in other sections of the fjord (Figs. 5 & 6). Along the
348 fjord sides, landforms from sediment reworking including slide scars, channels and gullies have
349 also been observed Fig 6b.

350 4.2.2. Linear Ridges Oriented Along Fjord Axis- Glacial Lineations

351 Oriented along the fjord's axis (or at times slightly oblique to it), linear features have been
352 identified in the inner and middle of the fjord, as well as a single lineation on the outer part of the
353 fjord (Figs. 5 & 6). They range in size from 100 to 1000 m in length and ~3 to 9 m in height,
354 although some that are as high as 80 m have been identified in the inner fjord. Their
355 morphologies vary throughout the fjord, and their length to width ratios range from 2:1 to 5:1.
356 Most ridges slope towards the outer fjord, although some slope in the opposite direction or have
357 an irregular or flat top. They appear both independently in connection with inferred bedrock
358 highs, and in clusters in flat lying areas of basin 3. These ridges have been interpreted as
359 glacial lineations, and they are thus indicating the direction of former glacier flow.

360 4.2.3. Transverse Ridges- Moraines

361 Several transverse ridges have been identified in the inner and central portion of the fjord,
362 oriented perpendicular to the fjord's axis (Figs. 2, 5 & 6). The ridges in the inner most position of
363 the fjord tend to largely conform to the topography (i.e., between bedrock mounds, some of
364 which are position mid-fjord (M4-6; Fig. 6b), and the fjord sidewalls) and are the threshold
365 between sub-basins (Fig. 6). The width and length of ridges range from 150 to 600 m and 120 to
366 500 m, respectively, where their heights are between <5 to 58 m.

367 A particularly large, asymmetrical transverse ridge that spans the width of the fjord, is situated
368 between Basin 3 and 4 (M3; Figs. 2 & 6d). This ridge is ~1.5 km in width and between 72 to 162
369 m in height. It contains a crescent shape in aerial view and is concave towards the mouth of the
370 fjord. A large threshold with a 1.8 km width and a > 215 m height also separates basin 1 and 2
371 (M1; Figs. 2 & 5). This feature is ~150m shallower in the north and dips steeply into basin 1.

372 The transverse ridges have been interpreted as moraines, which would have formed during
373 glacial stillstands or readvancements during the retreat of a grounded tidewater glaciers margin.
374 These moraines do not fill the width of the innermost fjord, which has also been seen in inner
375 Nordfjord (part of the Keiser Franz Josef fjord system) by Olsen et al. (2022). While the large
376 transverse ridge M3 is believed to be a moraine, it is considered more likely that M1 is a
377 bedrock mound based on its morphology. The smaller transverse ridges are interpreted as
378 recessional moraines. Smaller moraines have the potential to form at ice margins annually

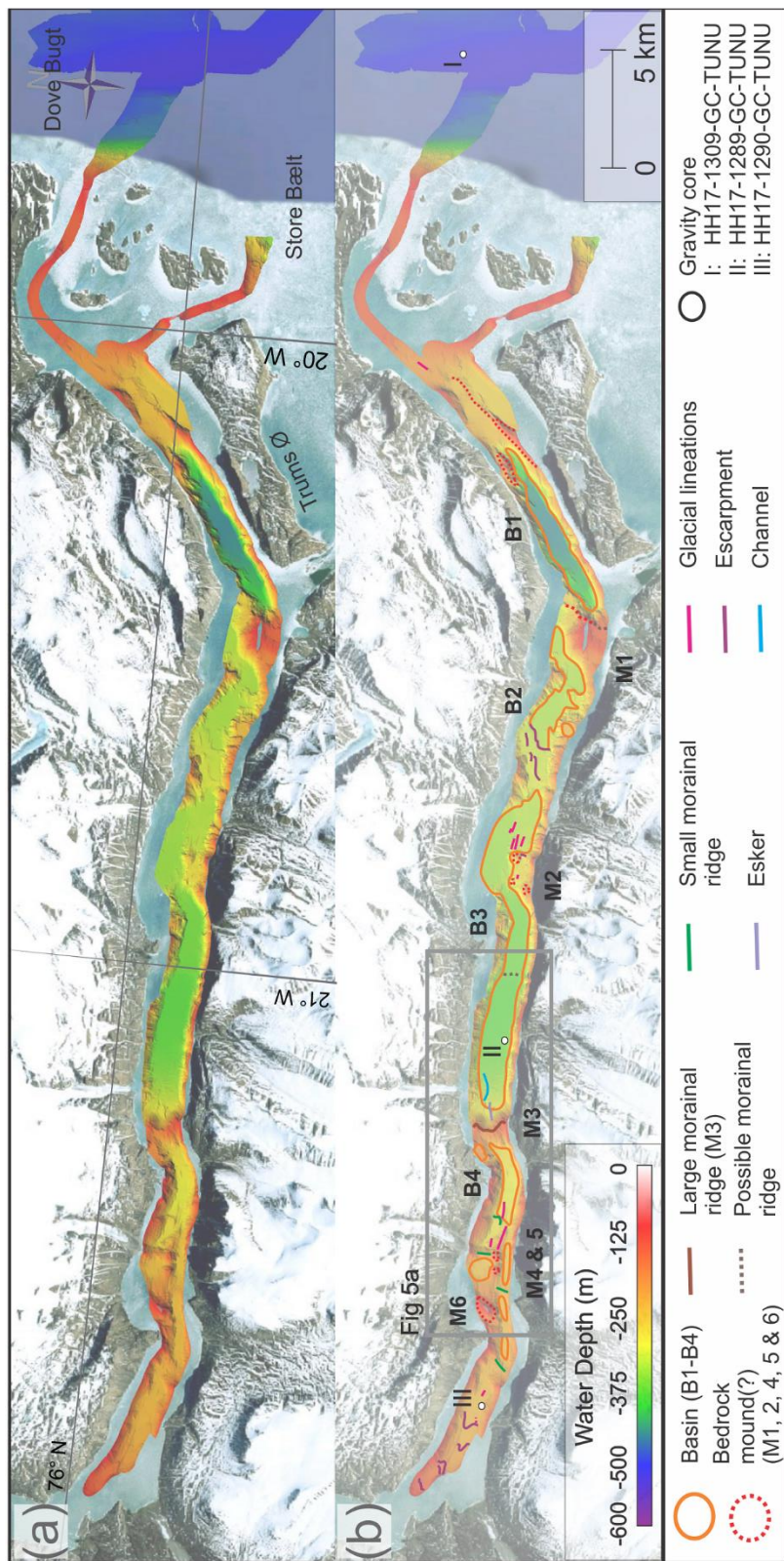
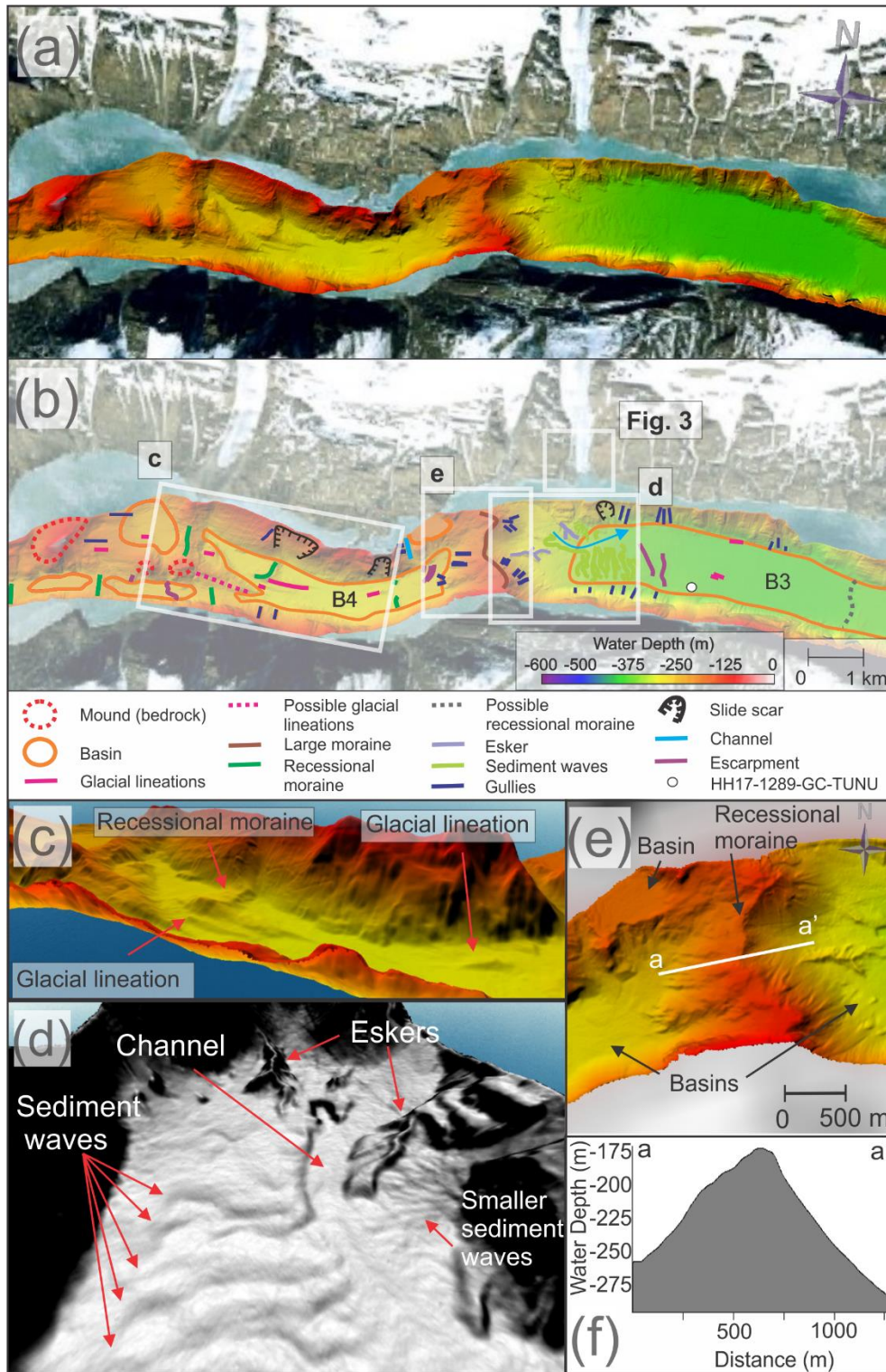


Figure 5. (a) Bathymetric map of Bessel Fjord. (b) A map of mapped features in Bessel Fjord. Satellite images obtained from Google Earth (© Google 2020).



381

382 Figure 6. (a-b) Mapped sections from inner to middle Bessel Fjord. Background images used for 6a & 6b obtained
383 from Google Earth (© Google 2020). (c) Glacial lineations in Basin 4 (B4). (d) Eskers, sediment waves and a channel
384 in Basin 3 (B3). (e) A large moraine (M3) between B3 and B4. Note the raised sub-basin to the west and esker to the
385 east. (f) Profile across the large recession moraine (M3).

386 (Lyså & Vorren, 1997; Dowdeswell et al., 2016) and have been observed with a variety of sizes
387 and morphologies on the NE Greenland shelf (e.g., Winkelmann et al., 2010).

388 *4.2.4. Sinuous Ridges- Eskers*

389 Sinuous ridges, oriented parallel or oblique to the fjord's axis, occur in basin 3 (Figs. 5, 6b, 6d
390 &6e). These features have widths and lengths of 50 to 120 m, 350 to 800 m, respectively and
391 heights of 10 to 15 m. The most pronounced examples of these ridges have been observed east
392 of the large recessional moraine that has been previously discussed (Fig. 6e).

393 These sinuous ridges have been interpreted as eskers. These landforms form from sediment
394 infill of subglacial and englacial conduits and have been identified in other studies in Greenland
395 (Huddart and Lister, 1981; Geirsdóttir et al., 2000; Winkelmann et al., 2010; Lane et al., 2015).
396 They frequently form in the direction of former ice flow and often form during terminal stages of
397 glaciation, and are therefore associated with moraines (Shreve, 1985). They vary in size
398 depending on the glacial drainage pattern, as well as a number of other factors, however eskers
399 identified within Bessel Fjord appear smaller than those identified in studies in Canada, the UK
400 and Kola Peninsula in Russia (Storrar et al., 2014).

401 *4.2.5. Wavy Transverse Ridges- Sediment Waves*

402 Adjacent to the two eskers in Basin 3 are a series of wavy transverse ridges to the east of a
403 large recessional moraine (Figs. 5, 6b & 6d). These features occupy an area of ~500 by 1500 m
404 and contain small ridges and flat areas that slope at an angle of 3 to 6° to the east. Each wave
405 "crest" is ~50 to 100 m apart, although some appear to begin only halfway through the width of
406 the area, where others occupy the entire width, north to south. These waves are crosscut by a
407 channel to the north (Fig. 6d). North of this channel similar features with a wavy morphology
408 occur, although these are substantially smaller.

409 These wavy transverse ridges have been interpreted as sediment waves. Sediment waves
410 found associated with deltaic and glacialfluvial deltaic systems have been associated with
411 retrogressive slope failures, gravity-induced sediment creep and/or the migration of sediment
412 waves upslope (Cartigny et al., 2011; Hill, 2012; Stacey and Hill, 2016). Alternatively, given the
413 position of the smaller wavy transverse ridges to the ice cap on Ad. S. Jensen Land (Figs. 1 &
414 2) and the larger ridges to the large moraine to the west (Figs. 5 & 6) it is also possible that
415 these ridges are sets of moraines. Recessional moraines have been identified in the vicinity of
416 eskers in Spitsbergen fjords (Ottesen et al., 2008; Kempf et al., 2013), which may account for
417 the smaller wavy transverse ridges. The larger wavy transverse ridge do also resemble thrust
418 moraines identified by Forwick et al. (2010). Further work may be required in the evaluation of
419 these features. For a full list of observed landforms see Table 4.

420 *4.3. Lithostratigraphy*

421 Three gravity cores were retrieved from the study area. Gravity core HH17-1309 was collected
422 in Store Bælt and was sampled from a N/NW-S/SE oriented depression that contains iceberg
423 ploughmarks and a MSGL. Gravity core HH17-1289 was collected in the middle of the Bessel
424 Fjord and is located directly east of the above-mentioned sediment waves on the distal part of
425 the pronounced transverse ridge. Nearby, a modern ice cap fed glacialfluvial channel is observed
426 in satellite imagery, likely with a delta at its fjord termination. The gravity core HH17-1290 was
427 collected within the inner fjord, west of the basins and thresholds observed in this study area
428 and is the closest core to Soranerbræen (located ~9.7 km east of the glacier) (Fig. 7).

429

430 Table 4. Overview of observed landforms in southern Dove Bugt and Bessel Fjord.

Region	Description	Width	Length	Height	Notable Feature	Interpretation
Dove Bugt	Elongated lineations	35-50 m	~1->10 km	<1-3 m	Roughly N-S	Glacial Lineations
	*Wide	200-650 m	3.8 to 8.8. km	4.5-15 m		
	Depression and mound	200 m	450 m	3-4 m	Mound to the south of the depression	Hill-hole pair
	Furrows (scour marks)	~40-100 m	<100-200	3-5 m	Irregular	Iceberg plough marks
	Transverse ridges	150-400 m	~30-100 m	0.5-1 m	Roughly W-E	Recessional moraines
Bessel Fjord	Linear ridge	45-350 m	100-1000 m	3-9, 80 m	Parallel to the fjord's axis	Glacial Lineations
	Transverse ridges	150-600 m	120- 500 m	<5-58 m	Perpendicular to the fjord's axis	Recessional moraines
	*Large ridge (M3)	1485 m	600-1600 m	72 to 162 m		Moraine
	Sinuuous ridges	50-120 m	350-800 m	10-15 m		Esker
	Wavy transverse ridges	400-700 m	~45-100 m	2-5 m	Perpendicular to the fjord's axis	Sediment wave
	Elongated depression	~200 m	~1 km	6-8 m		Channels
	Chute	~20-100 m	60-400 m	1-15 m		Gullies

431

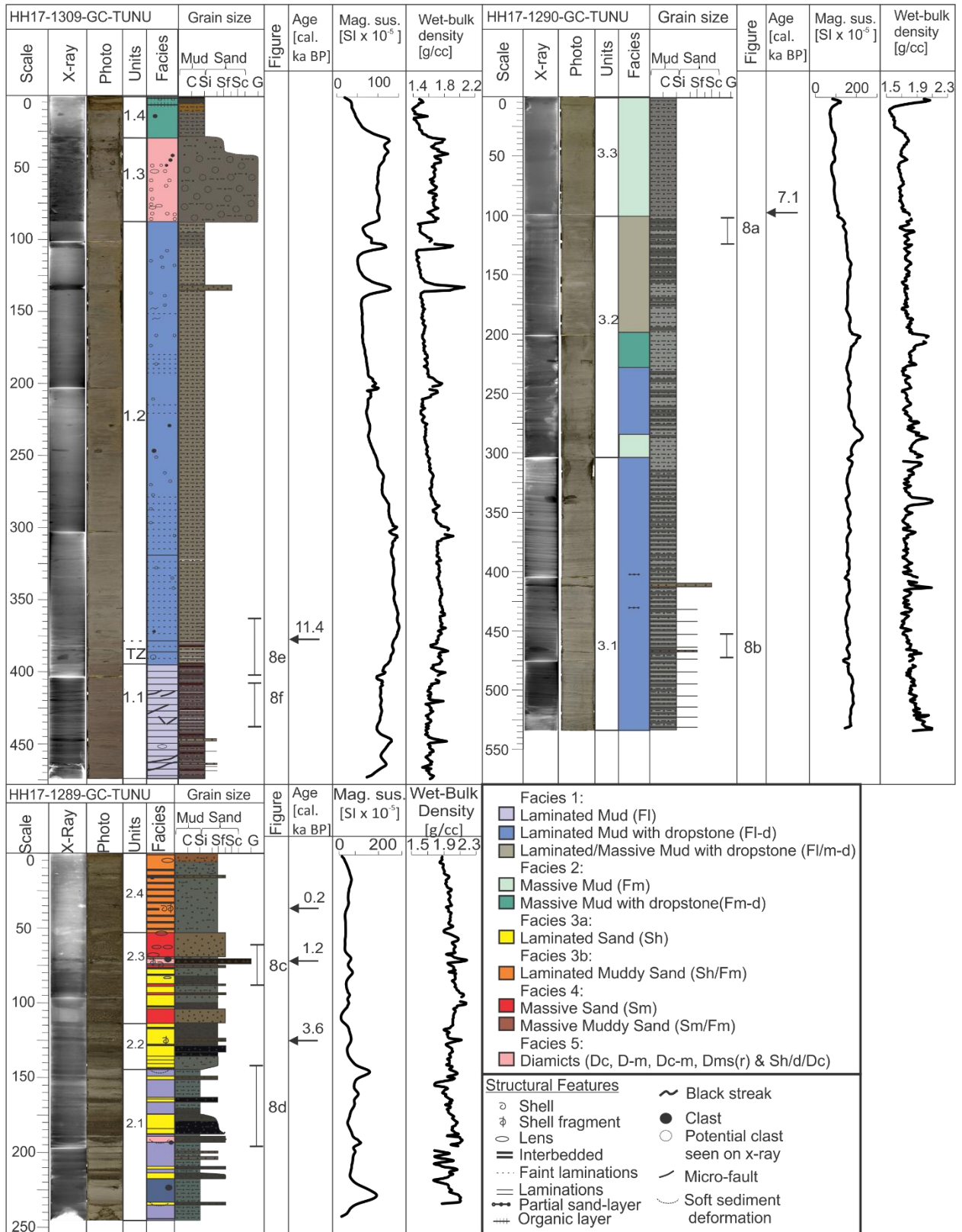
432 4.3.1. Facies

433 *Facies 1 – Laminated Mud (FI, FI-d & FI/m-d)*

434 Facies 1 consists of laminated mud (FI) and laminated mud with dropstones (FI-d) and have
 435 been observed in all three gravity cores (Figs. 7, 8a, 8d & 8f). Laminations are composed of
 436 either mud or very fine sand. Mud laminations with finer laminations have also been identified in
 437 Unit 3.2 (100-200 cm; Fig. 7a, FI/m-d). Microfractures have also been identified within this facies
 438 (Fig. 8f).

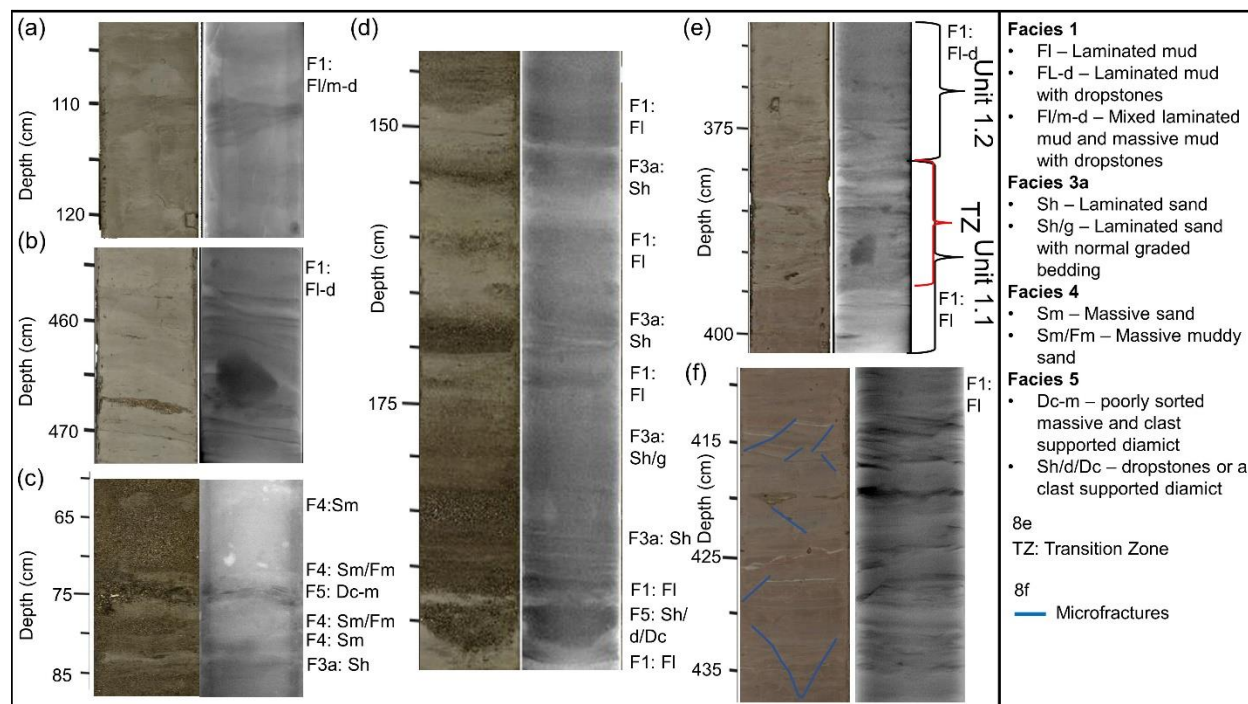
439 Wet-bulk density measurements tend to increase with depth in some sections of this facies
 440 (e.g., 87-350 cm in HH17-1309), suggesting normal sediment consolidation. However, a
 441 stagnation or decrease in wet-bulk density with depth in other sections (e.g., below ~350 cm in
 442 HH17-1309) suggests less consolidation. The magnetic susceptibility generally tends to
 443 increase with depth in HH17-1309 and in Unit 3.2 in HH17-1290, however the remainder of this
 444 facies in HH17-1290 (Unit 3.1) remains relatively stable to the base of the core. Notable positive
 445 peaks have been identified at 110 and 140 cm in HH17-1309 and measurement fluctuations
 446 occur in HH17-1289. Peaks in magnetic susceptibility may reflect the introduction of turbidites or
 447 clasts where fluctuations may reflect shifts in sediment provenance.

448 Muds with sand laminations are believed to have formed through a combination of ice-proximal
 449 suspension settling from overflow plumes and turbidity-current activity (underflows). The
 450 rhythmically laminated muds are believed to have formed from ice-proximal suspension settling
 451 from turbid overflow plumes. Similar laminated sediments have been identified in Kejsler Franz
 452 Joseph Fjord and Fosters Bugt in East Greenland and are theorized to have been deposited



453

454 *Figure 7. Lithological core logs of the three gravity cores with x-ray images, core photos, unit divisions, facies,*
 455 *structures, magnetic susceptibility, and wet-bulk density. TZ in HH17-1309-GC-TUNU stands for “Transition Zone”.*
 456 *Grain size abbreviations: C: clay, Si: silt, Sf: fine grained sand, Sc: coarse grained sand and G: gravel.*



458

459 *Figure 8. Photographic and x-ray images of sections of the three gravity cores (a-f). Corresponding facies codes can*
 460 *be found to the right of each image.*

461 from turbid meltwater plumes in an ice-proximal environment (Evans et al., 2002). Large clasts
 462 have been interpreted as ice rafted debris (IRD). The formation of microfractures may have
 463 been caused by soft sediment deformation, possibly from grounded icebergs.

464 *Facies 2 – Massive Mud (Fm & Fm-d)*

465 The second facies consists of massive mud with or without dropstones and can be found in the
 466 inner fjord core HH17-1290 and the Store Bælt core HH17-1309 (Fig. 7). In HH17-1290 this
 467 appears downcore between sections of Facies 1 as well as in the topmost unit, Unit 3.3. The
 468 magnetic susceptibility gradually increases downcore in this facies in Unit 3.3. Further down
 469 core, in Unit 3.2, this facies is associated with a downwards trend in magnetic susceptibility
 470 following peaks in measured readings. Wet bulk density values roughly mirror these trends. In
 471 HH17-1309 massive mud units have been observed in Unit 1.4, where magnetic susceptibility
 472 and wet bulk density values increase downcore.

473 This facies is interpreted as being the result of suspension settling from overflow plumes and is
 474 believed to have been deposited in an ice-distal glacial marine environment with varying input from
 475 IRD (i.e., Boulton & Deynoux, 1981). Sediment may be sourced from a single location (i.e.,
 476 Soranerbræen) or more than one location (e.g., local ice caps) in an ice-distal glacial marine
 477 environment with limited iceberg or sea-ice rafting. Massive mud deposits have also been
 478 identified in other Greenland fjords (e.g., Ó Cofaigh et al., 2001) and it has been suggested that
 479 they may indicate meltwater from ice- or fjord margin-distal conditions (Evans et al., 2002).

480 *Facies 3a – Laminated Sand (Sh)*

481 Facies 3a consists of sections of sand with horizontal sand laminations. This facies has been
482 predominantly observed in the mid-fjord core, HH17-1289-GC-TUNU (Figs. 7 & 8d). These
483 sections consist of fine to medium grained sand that range in thickness and colors. Occasionally
484 this facies also contains normal graded bedding (e.g., Fig. 8d, ~174-183 cm). This facies does
485 not contain uniform magnetic susceptibility or wet-bulk density readings as it has been found in
486 association with low and high peaks of both parameters as well as values that are near the
487 average for the core.

488 This facies is interpreted as being deposited from turbidity currents, possibly underflows that are
489 either sourced from glacial or non-glacial streams and slope failures. Uniform layers may
490 indicate a single, rapid event, where shifts in grain size and color may be the result of short-lived
491 fluctuations in sediment input. Laminated sands have been identified in Scoresby Sund in East
492 Greenland and have also been attributed to turbidite formation (Ó Cofaigh et al., 2001).

493 *Facies 3b – Laminated Muddy Sand (Sh/Fm)*

494 Facies 3b represents sections of sand with faint horizontal laminations as well as a large
495 quantity of clay material interspersed throughout with faint laminations. This has been observed
496 in HH17-1289 at the topmost unit in the core, Unit 2.4 (Fig. 7). Magnetic susceptibility is
497 relatively uniform in this facies, where the wet-bulk density tends to decrease up core. Sediment
498 grain size analysis of a single sample from this facies revealed that the sediment is composed
499 of 56.3% sand and 43.7% mud. A “patch” of black organic material (i.e., plant material and
500 shells) was also identified within this unit.

501 This complex facies is believed to have formed predominantly from underflow events, sandy –
502 muddy turbidites, alternatively sandy turbidites with additional input from suspension settling.
503 Similar deposits have been observed in Balsfjord, Norway although without lamination and
504 possibly a higher mud content (Forwick and Vorren, 1998).

505 *Facies 4 – Massive Sand / Massive Muddy Sand (Sm & Sm/Fm)*

506 Facies 4 contains sections of massive sand (Sm) as well as massive sand with a large amount
507 of clay content (Sm/Fm). This facies is predominantly found in Unit 2.3 (and to a much less
508 extent, Unit 2.4) in HH17-1289 (Fig. 7). Sections of massive sand have been found in
509 association with mud lenses and often contain horizontal sand layers (Sh) above and below it.
510 Slight increases and decreases in magnetic susceptibility values have been observed within this
511 facies.

512 This facies is believed to have developed through rapid deposition as well as deformation of
513 Facies 3a & b. According to this interpretation, the mud lenses observed in this facies were
514 once layers/lamina that became deformed due to the sand – mud density contrast. Massive
515 sand has been found in Kangerlussuaq and Miki Fjords in East Greenland (Smith and Andrews,
516 2000) and well-sorted coarse grain deposits have been recovered near Petermann Glacier in
517 northern Greenland (Reilly et al., 2019). Authors have attributed these layers to sediment gravity
518 flows.

519 *Facies 5 – Diamicts (Dc, D-m, Dc-m, Dms(r) & Sh/d/Dc)*

520 Facies 6 contains a variety of different diamicts observed within the mid-fjord core HH17-1289
521 and the Store Bælt core HH17-1309. In HH17-1289 this includes a 3.5 cm poorly sorted
522 massive, and clast supported diamict (Dc-m) in the middle of Unit 2.3 (Figs. 7 & 8c), and a
523 horizontally laminated layer of sand that that is either accompanied by dropstones or a clast

524 supported diamict (Sh/d/Dc) (Figs. 7 & 8d). It is inferred that they are the result of sea ice or
 525 iceberg rafting/dumping. Within HH17-1309 there is a substantially larger, sharp based, matrix-
 526 supported diamict, stratified in its upper part (Dms(r)) in Unit 1.3 (Fig. 7). Based on these
 527 characteristics, this diamict has been interpreted as a density flow deposit, likely a debris flow
 528 deposit that is overlain by (part of) a turbidite.

529 4.3.2. Core chronology

530 Shell and shell fragments were recovered from HH17-1289 for radiocarbon dating. At 34 cm
 531 depth, a semi-spherical path of organic content was identified, containing two intact *Yoldiella*
 532 *lenticula*, a shell fragment and plant material. Additionally, at 71 cm depth, a large 3 cm half of a
 533 *Hiatella arctica* shell was collected for dating, and shell fragments were recovered from a depth
 534 of 125 cm for the same purpose. These shells yielded radiocarbon ages of 0.2, 1.2 and 3.6 cal.
 535 ka BP, respectively (Table 5).

536 Cores HH17-1290 and HH17-1309 were subsampled for foraminifera material at four positions
 537 and calcareous benthic species were used for dating. In HH17-1290 this included predominantly
 538 *Melonis barleeanus* and small amounts of *Islandiella norcrossi*. In HH17-1309, at a depth of 377
 539 cm *Islandiella norcrossi* (rare to common), *Stainforthia feylingi* (rare) and a planktonic species
 540 were identified immediately above the transition zone between two facies. Radiocarbon dates
 541 for the HH17-1309 sample yielded an age of 11.4 cal. ka BP where the sample from HH17-1290
 542 yielded an age of 7.1 cal. ka BP (Table 5).

543 Table 5. Calibrated radiocarbon dates.

Coring station	Sampling Depth [cm]	Lab nr.	Species	¹⁴ C age BP	Marine20 cal BP (1σ range)	Marine20 cal BP
HH17-1309-GC-TUNU	377	5157.1.1	Mixed benthic foraminifera	10357 ± 95	11201 - 11553	11386
HH17-1289-GC-TUNU	35	5154.1.1	<i>Yoldiella lenticula</i>	688 ± 34	61 - 253	158
HH17-1289-GC-TUNU	71	5155.1.1	<i>Hiatella arctica</i>	1747 ± 28	1065 - 1250	1152
HH17-1289-GC-TUNU	125.5	5156.1.1	Bivalve frag.	3809 ± 36	3472 - 3701	3596
HH17-1290-GC-TUNU	97	5158.1.1	Mixed benthic foraminifera	6800 ± 80	6990-7250	7116

544

545

546 **5. Discussion**

547 **5.1. *Ice Sheet advance***

548 The appearance of glacial lineations in Bessel Fjord suggest that the fjord was once fully
549 glaciated, which is in accordance with the inferred shelf break-terminating ice sheet inferred for
550 the LGM from other studies (e.g., Laberg et al., 2017; Olsen et al., 2020) (Figs. 9a & 9b). Ice
551 that filled the fjord is believed to most likely be from the modern Soranerbræen glacier but may
552 have also included ice caps and other nearby branches of inland ice.

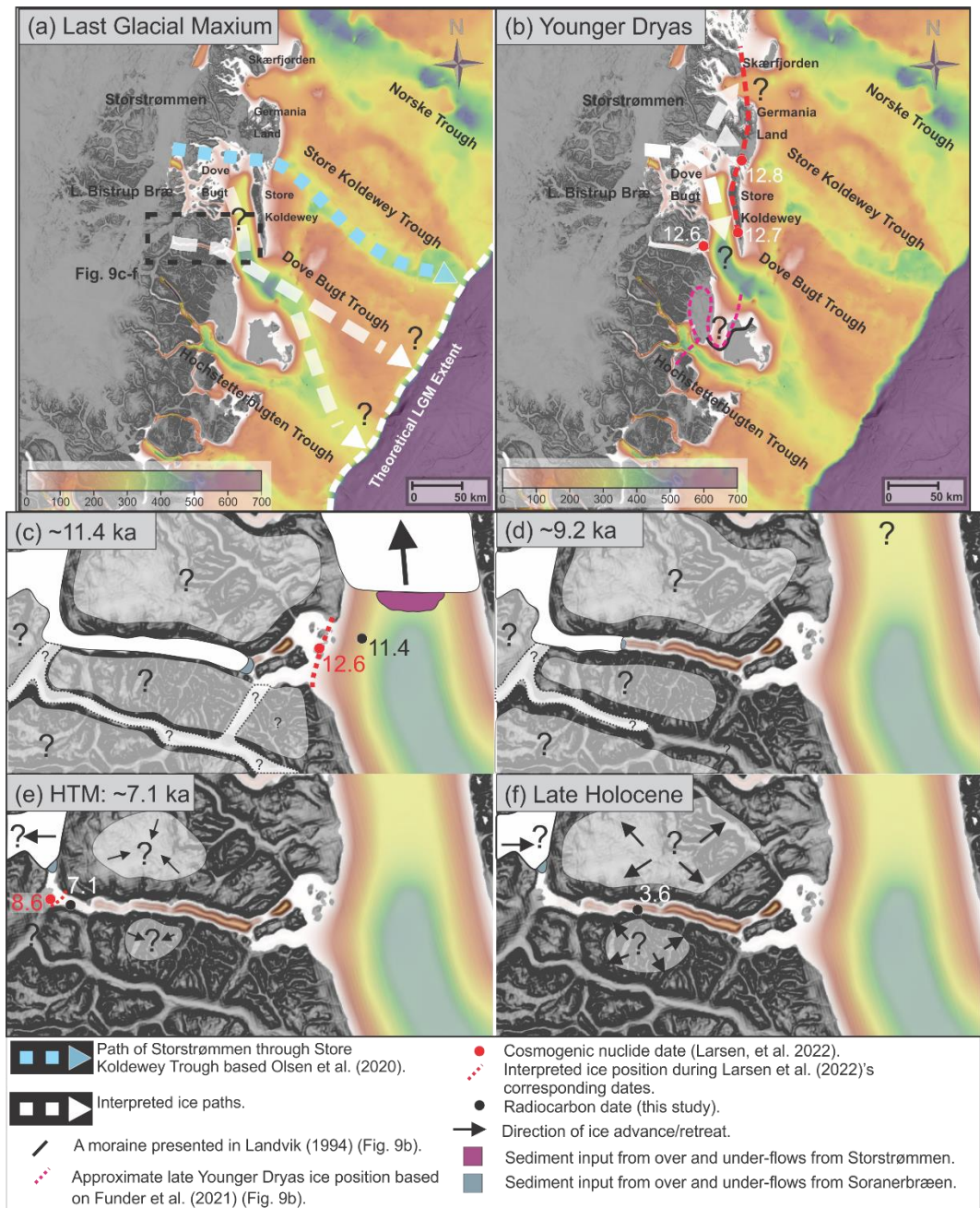
553 Glacial lineations are believed to have formed during the LGM but could have also formed
554 during an ice readvance in the deglaciation (see below). Onshore and south of Bessel Fjord,
555 two sets of striations identified in Langsødalen (Hjort, 1979, 1981) may suggest that this valley
556 experienced two glaciation events (Fig. 1c). Striations, and lateral moraines, found along the
557 fjord axis may be the result of the east-west movement of ice through the valley, where SW
558 oriented striations may be the result of Storstrømmen encroaching also onto terrestrial areas.
559 Hjort (1981) suggested that striae on Haystack may indicate that ice flow was dominant from the
560 north during the Nanok Stadial but ice pressure from Langsødalen dominated later after
561 deglaciation begun. Thus, it is possible that ice masses drained through both Bessel Fjord and
562 Langsødalen during full-glacial conditions further advancing into Dove Bugt/Store Bælt.

563 In Store Bælt, the orientation of glacial lineations (e.g., MSGs) suggest that ice flowed to the
564 south along the west coast of Store Koldewey, marking the southwards expansion of the
565 Storstrømmen ice stream (Figs. 9a & 9b). East of Dove Bugt, MSGs identified in Store
566 Koldewey Trough are believed to have formed when the Storstrømmen ice stream acted as a
567 “pure” ice stream (Bentley, 1987; Stokes and Clark, 1999) and overrode the underlying
568 topography during the LGM (Fig. 9a; Olsen et al., 2020). It was theorized that at a later phase,
569 when the ice sheet began to thin, the ice stream became more influenced by the topography of
570 deep troughs, draining northwards to Jøkelbugten and southwards to Dove Bugt (Olsen et al.,
571 2020). Assuming these two phases occurred in the Storstrømmen ice stream development, it is
572 possible that these glacial lineations in Store Bælt represent a period when a branch of the ice
573 stream began conforming to topographical controls (e.g., Store Koldewey) and flowed towards
574 the south. At this point the ice may have flowed into the southeast through Dove Bugt Trough
575 (Fig. 9a).

576 An alternative interpretation, that cannot be excluded, is that these MSGs formed during a
577 glacial re-advance that followed the LGM. Between Hochstetter Forland and Shannon Ø a
578 submerged moraine has been identified in Shannon Sound, which may indicate that at one point
579 the ice stream travelled south rather than through Dove Bugt Trough (Figs. 9b & 10a; Hjort,
580 1981; Landvik, 1994; Larsen et al., 2016; Funder et al., 2021). However, constraints from Store
581 Koldewey, Germania Land and Trums Ø, do not support an ice advance during the Younger
582 Dryas (Fig. 10b; see below). The formation of the submerged moraine was possibly due to an
583 ice readvance of the GrIS outlet(s) (Soranerbræen, L. Bistrup Bræ and/or Storstrømmen)
584 through western, inner Dove Bugt (Fig. 9b), where the surroundings (onshore and offshore)
585 were not or less affected. If this is correct, the readvance may have occurred during the
586 Younger Dryas (prior to 11.4 cal. ka BP, see below).

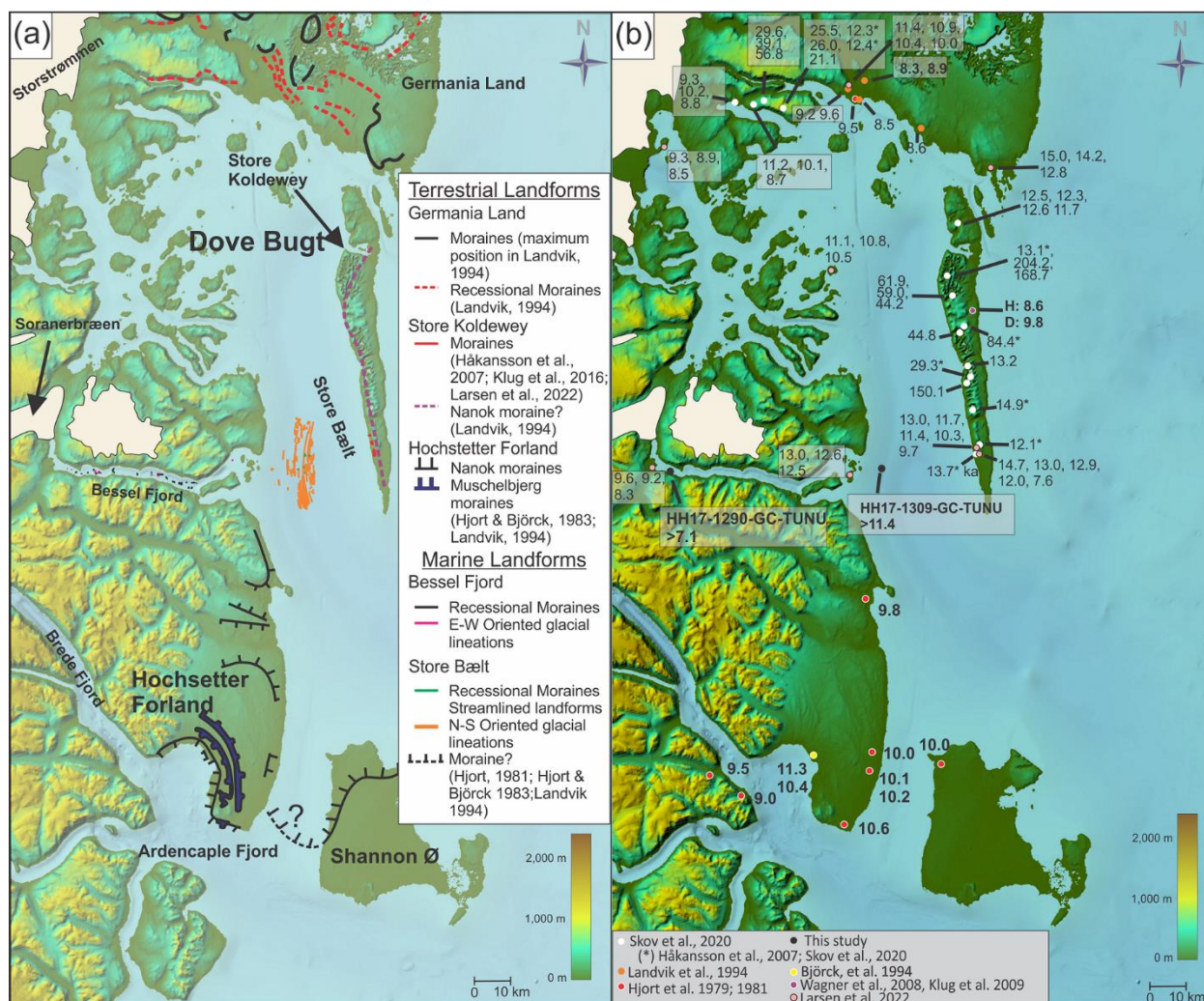
587 **5.2. *Ice Sheet retreat through Store Bælt***

588 The deglaciation age of 11.4 cal. ka BP (Table 5) from Store Bælt immediately east of the
589 Bessel fjord entrance is attributed to the retreat of a N-S bound branch of the NEGIS (Fig. 9c)



590

591 *Figure 9. Maps showing ice sheet extent and advancement/retreat directions in SW Dove Bugt and Bessel Fjord*
 592 *during a range of periods. (a) The interpreted position of the ice sheet during the LGM. (b) The theoretical position of*
 593 *ice in Bessel Fjord and Dove Bugt during the Younger Dryas. (c) The ice position in Bessel Fjord at ~11.4 ka based*
 594 *on approximated deglaciation date presented in this study and the position and radiocarbon date for gravity core*
 595 *HH17-1309. The size of ice caps in c-f are only indicative. (d) The position of ice in Bessel Fjord at ~9.2 ka based on*
 596 *approximated deglaciation data from this study. (e) Ice retreating beyond our gravity core (HH17-1290) at ~7.1 ka*
 597 *during the HTM. (f) The Late Holocene ice expanse in Bessel Fjord with a radiocarbon date from gravity core HH17-*
 598 *1289. Background bathymetry displayed using IBCAO data (Jakobsson et al., 2020).*



600
601 *Figure 10. (a) Marine moraine ridges and glacial lineations from the current study together with previously mapped*
602 *marine and terrestrial features. (b) Location of deglaciation dates from this study (Table 5) and previous publications.*
603 *See Table 3 for recalibrated radiocarbon dates. H: Hjort Lake, D: Duck Lake. Background displayed using IBCAO*
604 *data (Jakobsson et al., 2020).*

605 due to the presence of N-S oriented glacial lineations near the gravity core. This date represents
606 a minimum age for the deglaciation as it is not from the base of the deglacial deposits.
607 Previously published dates constraining the timing of deglaciation in Dove Bugt have been
608 restricted to terrestrial regions (Fig. 10b). Using cosmogenic nuclide dating, Skov et al., (2020)
609 produced deglaciation ages of ca. 12.7 ka at Store Koldewey and ca. 9.8 ka at Pusterdal and
610 later Larsen et al. (2022) produced a number of deglaciation ages across Dove Bugt and Bessel
611 Fjord (8.6-12.8 ka) (Fig. 10b).

612 Our minimum age of ~11.4 cal. ka BP from HH17-1309 largely matches findings in Dove Bugt
613 and Hochsetter Forland (Fig. 10b). It is slightly later than average cosmogenic nuclide ages
614 obtained from Larsen et al. (2022) on Trums Ø (12.6 ka) and a Nanok moraine on southern
615 Store Koldewey (12.7 ka), but earlier than a second Store Koldewey Nanok moraine (11.0 ka)
616 as well as positions closer to the modern ice margin of Storstrømmen, such as Licht Ø (10.8 ka)

617 and Bræ Øerne (8.9 ka). Thus, Store Koldewey, and Trums Ø may have been partially
618 deglaciaded slightly prior to the final retreat of the NEGIS through Store Bælt.

619 Radiocarbon dates obtained from lake sediments on Store Koldewey suggest that the earliest
620 onset of warmth may have begun ~10 cal. ka BP (Klug et al., 2009), therefore, the deglaciation
621 of the area beginning prior to this may further support these results. Additionally, Landvik (1994)
622 produced a range of deglaciation ages between 9.6 to 8.5 cal. ka BP along the northern coast of
623 Dove Bugt (Hvalrosodden and Snenæs on Germania Land) and Hjort (1981, 1979) provided a
624 range of deglaciation ages between 10.6 to 9.8 cal. ka BP on Hochstetter Forland. Later Björck et
625 al. (1994), on Hochstetter Forland, dated *Hiatella arctica* shells near the shore of Peters Bugt
626 Sø and *Portlandia arctica* shells in a delta distal to a Nanok I ridge to 10.4 and 11.3 cal. ka BP,
627 respectively (Table 3; Fig. 10b).

628 Although based on a limited data set, the lack of prominent morainal landforms in Store Bælt
629 may also suggest a rapid retreat through the region. A small number of retreat moraines have
630 been observed in an isolated region of the study area, but the most prominent geomorphic
631 landforms are glacial lineations. Placing Store Bælt within the context of Dowdeswell et al.
632 (2008)'s proposed model for ice streams in high latitudes, ice likely retreated through the area
633 rapidly, although the presence of small moraines may suggest brief periods of stagnation. This
634 is in accordance with findings by Larsen et al. (2020, 2022) that deep fjords and outer regions in
635 eastern North Greenland were rapidly deglaciaded between ~12.6 and 10 ka. However,
636 additional data is required to confirm this.

637 Oceanic warming is believed to have contributed to the deglaciation of the inner shelf further
638 north and south of Dove Bugt (e.g., Jackson et al., 2022; Davies et al., 2022). Within the study
639 area, Store Koldewey does largely block oceanic water from the shelf from entering Store Bælt,
640 however, it is possible that warmer water traveled through the Dove Bugt Trough to the south
641 and impacted a north-south branch of the ice stream. This mechanism for warm water transport
642 has also been suggested for other east Greenland troughs (Arndt et al., 2015) and used to
643 explain how warm water has reached other outlets of the NEGIS (e.g., Zachariae Isstrøm via
644 the Norske Trough (Schaffer et al., 2017)).

645 5.3. *Ice sheet retreat through Bessel Fjord*

646 Cosmogenic nuclide dates from Trums Ø suggest that the deglaciation of the outer fjord began
647 around 12.6 ka (Larsen et al., 2022). Gravity core HH17-1290, collected from the inner fjord
648 region, consists of sediments that reflect an increasingly ice distal environment up core. One
649 radiocarbon date from the core provides a minimum age of ~7.1 cal. ka BP for the deglaciation
650 of Soranerbræen and/or local ice caps from the inner fjord region (Table 5 & Fig. 9e). This date,
651 however, is not from the base of the deglacial deposits and therefore represents a minimum age
652 for the deglaciation of the inner fjord. New cosmogenic nuclide dates from Vandrepasset
653 (onshore innermost Bessel fjord area, connecting the fjord and the next valley to the south)
654 provide an age of 8.6 ka for the deglaciation of the innermost fjord area (Larsen et al., 2022),
655 confirming this interpretation. Our minimum age of 7.1 cal. ka BP and the results of Larsen
656 (2022) falls within a modelled ice sheet extent by Lecavalier et al. (2014) which placed the
657 position of the ice sheet in the middle of Bessel Fjord at 9 cal. ka BP and that the present-day
658 ice margin is reached by 6 cal. ka BP. The minimum age also agrees with the onset of HTM on
659 Store Koldewey (~8.0 to 4.0 cal. ka BP) (Wagner et al., 2008; Klug et al., 2009; Schmidt et al.,
660 2011) and Hochstetter Forland (8.8 and 5.6 cal. ka BP) (Björck & Persson, 1981; Björck et al.,
661 1994). Thus, the GrIS retreated from the marine realm in Early Holocene, slightly before or at

662 the time of the HTM in this region (characterized by a mean July temperature 2-3°C higher than
663 at present; Bennike et al., 2008).

664 The appearance of recessional moraines in Bessel Fjord suggests that the fjord underwent a
665 stepwise deglaciation. The large moraine identified between Basin 3 and Basin 4 (M3; Fig. 7e)
666 is believed to have formed during a major ice halt or readvance, possibly climatically induced.
667 Smaller moraines occasionally follow topographic boundaries, which may suggest that the
668 retreat of ice in Bessel Fjord was also partly topographically controlled. Recessional moraines
669 identified by Olsen et al (2020) east of Dove Bugt in Store Koldewey Trough contain similar
670 heights to those identified here (excluding M3). However, there are more moraines identified in
671 Store Koldewey Trough than in Bessel Fjord, and they are wider, which is likely due to the lack of
672 topographic confinement.

673 A decrease in atmospheric temperatures in early Holocene is recorded in the Greenland
674 Summit temperature records and includes the Preboreal Oscillation and the 9.2 ka event
675 (Kobashi et al., 2017). We tentatively suggest that some of the moraines identified in the Bessel
676 fjord may have developed during some of these events. From this we suggest that increased
677 Northern Hemisphere summer insolation that peaked in the early Holocene was the main
678 control for this part of the deglaciation during which the ice front receded from the coastline to
679 the west of (onshore) Bessel Fjord, a distance of ~60 km. Assuming that this occurred over a
680 maximum period of ~4.3 cal. ka BP (11.4-7.1 cal. ka BP, see discussion above on the timing
681 and length of this period), this corresponds to an average minimum ice recession rate of ~14
682 m/yr. Further supporting this average rate, if one applies this same approach to the two average
683 Bessel Fjord cosmogenic nuclide dates presented by Larsen et al. (2022) (12.6-8.6 ka) and the
684 distance between their sampling locations (~56 km), it also results in a rate of 14 m/yr. This rate
685 is considered realistic as it is half (or less) than the rate estimated from the
686 Nioghalvfjærsfjorden further north (also part of the Storstrømmen ice stream) where a rate of
687 ~30-40 m/yr was reported (Bennike & Björck, 2002). This rate places Soranerbræen near the
688 large moraine M3 around the 9.2 ka event (Fig. 9d).

689 While oceanic warming may be partially responsible for the retreat of the NEGIS through Store
690 Bælt, we believe that Bessel Fjord is too sheltered by the sill at its entrance to have allowed
691 warm, intermediate water to enter and make a significant impact of the deglaciation of the
692 southern outlet of Soranerbræen. Our bathymetric dataset reveals that the depth of the sill is
693 between ~50 to 200 m, however large parts of it are above water and form islands. This is far
694 shallower than other fjord sills in the region that are theorized to have blocked warm Atlantic
695 Water (e.g., the sill in Dijnphna Sund to the north, which has a maximum depth of 170 m
696 (Wilson and Straneo, 2015)). Also, the effect of the glacio-eustatic readjustment is considered to
697 be small for this region, ~9.5 m higher in the Young Sound region (slightly south of our study
698 area) 7500 years ago (Pedersen et al., 2011). Rignot et al. (2022) also theorized that seafloor
699 topography may impact whether warm water is reaching the northern outlet of Soranerbræen.
700 They suggested further that the grounding line retreat of Storstrømmen, L. Bistrup Bræ, and
701 possibly Soranerbræen, may primarily be caused by ice thinning from atmospheric warming
702 (Rignot et al., 2022). We suggest that a similar mechanism may be responsible for
703 Soranerbræen's retreat through Bessel fjord during the deglaciation.

704 **5.4. Holocene glacier variability and sedimentary processes in Dove Bugt**
705 Sedimentological evidence (e.g., ice-proximal laminated muds) from HH17-1309 suggests, that
706 suspension settling from a glacial source(s) likely dominated southwestern Dove Bugt during the

707 Holocene. The contribution of sediment from the NEGIS seems unlikely, as Pusterdal became
708 deglaciated by 9.5 ka (Skov et al., 2020) and Storstrømmen retreated beyond Bræ Øerne by 8.9
709 ka (Larsen et al., 2022), therefore it very well may be from Soranerbræen, or local ice caps.

710 During the latter part of the HTM in the middle Holocene, a time period in which some glaciers
711 are believed to have reached their minimum extent across Greenland, the NEGIS is believed to
712 have retreated beyond its current position between 5.4 to 1.2 cal. ka BP (Table 3), creating the
713 Storstrømmen Sound (Weidick et al., 1994). Laminations appear less frequently in the upper
714 part of core HH17-1309, yet they are not absent. Laminations are entirely absent in the Bessel
715 Fjord core HH17-1290 during this period and remain absent through the colder Late Holocene.
716 Later, during the Little Ice Age, Storstrømmen has demonstrated to have expanded to its
717 modern day position (Weidick et al., 1994).

718 Gravity core HH17-1289, collected to the north of an onshore glaciofluvial channel connected to
719 a modern-day ice cap, transitions to complex assortment of sand layers just prior to 3.6 cal. ka
720 BP (Fig. 7). Sedimentological evidence suggests that these sand layers are largely the result of
721 rapid, short lived depositional events (i.e., turbidity currents) interpreted to be related to the
722 growth of a delta slightly south of the core site, from glaciofluvial sediment input from a nearby
723 outlet glacier.

724 Pollen assemblage data from Hochstetter Forland mark the end of the HTM at 5.6 cal. ka BP
725 (Björck and Persson, 1981; Björck et al., 1994) and information derived from aquatic organisms
726 mark the end of the HTM on Store Koldewey at 4 cal. ka BP (Wagner et al., 2008; Klug et al.,
727 2009b; Schmidt et al., 2011). This coincides with the onset of turbidites in core HH17-1289.
728 Therefore, it is possible that this shift to sand dominated sedimentation within this core was
729 controlled by climatically driven processes. This onset is here suggested to result from higher
730 sediment input through the channel as local ice caps expanded outwards following the HTM,
731 possibly in response to this climate cooling (Fig. 9f). This period of cooling also corresponds to
732 extended concentrations of sea ice on the shelf (Kolling et al., 2017).

733 **6. Conclusion**

734 In summary:

- 735 • Glacial lineations (MSGLs) identified in SW Dove Bugt suggest fast-flowing ice,
736 interpreted to be from the NEGIS, developed during the LGM or an ice readvance during
737 the deglaciation.
- 738 • Our minimum deglaciation date for Store Bælt (>11.4 cal. ka BP) is slightly younger than
739 new cosmogenic nuclide dates found onshore on Trums Ø and one of two Nanok
740 stadials on Store Koldewey (Larsen et al., 2022) as well as various other dates across
741 Store Koldewey (e.g., Skov et al., 2020). Thus, Store Koldewey and Trums Ø may have
742 been partially deglaciated prior to the final retreat of the NEGIS through Store Bælt.
- 743 • Moraines in Bessel Fjord (to the west of Dove Bugt) suggests that the fjord underwent
744 multiple halts/or readvances upon deglaciation. Thus, the bathymetry of Bessel Fjord
745 indicates that the glacial dynamics of the fjord were more dynamic than onshore
746 evidence suggests.
- 747 • The radiocarbon date of 7.1 cal. ka BP obtained in an inner fjord core is interpreted as a
748 minimum age at which Soranerbræen retreated to or beyond its present-day onshore

749 position west of the fjord and is in conformity with cosmogenic nuclide dates presented
750 by Larsen et al. (2022) in the onshore inner fjord (8.6 ka).

- 751 • An average ice recession rate in Bessel Fjord was determined to be ~14 m/yr using data
752 from this study as well as cosmogenic nuclide dates from Larsen et al., (2022).
- 753 • The GrlS retreated from the marine realm in the early Holocene, around the time of the
754 onset of the HTM in this region. From this we suggest that increased Northern
755 Hemisphere summer insolation that peaked in the early Holocene was the main control
756 for this part of the deglaciation.
- 757 • Sedimentological evidence after 7.1 cal. ka BP in HH17-1289 (i.e., the presence of only
758 massive mud) suggests that Soranerbræen did not expand back into Bessel Fjord for the
759 remainder of the Holocene.
- 760 • The transition of mud to muddy sand at 4 cal. ka BP in a mid-fjord core HH17-1289 may
761 provide evidence for local ice cap growth. Thus, ice caps in Bessel Fjord may have
762 fluctuated with greater sensitivity to climatic conditions than the NE sector of the GrlS
763 during the cooling phase that followed the HTM.

764

765 *Data availability:* The bathymetry and core data from UiT The Arctic University of Norway will be
766 available upon reasonable request at UiT's open research data repository:
767 <https://dataverse.no/dataverse/uit>.

768 *Author contributions:* Jan Sverre Laberg and Tom Arne Rydningen designed this study and
769 collected the new data during the 2017 TUNU VII cruise. The bathymetrical and lithological data
770 were interpreted by Kevin Zoller in collaboration with Jan Sverre Laberg and Tom Arne
771 Rydningen. Kevin Zoller prepared the manuscript with contributions from all co-authors.

772 *Competing interests:* The authors declare that they have no conflict of interest.

773 *Acknowledgement:* We would like to thank the participants of the 2017 TUNU cruise to
774 Greenland for making this project possible. A special thanks to the captain and crew of the RV
775 *Helmer Hanssen* for their involvement in the cruise and assistance in collecting the data. A
776 thanks also goes out to the lab staff at UiT, Trine Dahl, Karina Monsen and Ingvild Hald, who
777 assisted with processing sediment core samples for this project. We would also like to thank
778 Gesine Mollenhauer and the lab staff at the Alfred Wegener Institut for providing us with
779 radiocarbon dated material using their MICADAS. Funding for this work was provided by UiT
780 The Arctic University of Norway.

781

782 **References**

783 Arndt, J. E.: Marine geomorphological record of Ice Sheet development in East Greenland since
784 the Last Glacial Maximum, *J. Quat. Sci.*, 33, 853–864, <https://doi.org/10.1002/jqs.3065>, 2018.

785 Arndt, J. E., Jokat, W., Dorschel, B., Mykleburst, R., Dowdeswell, J. A., and Evans, J.: A new
786 bathymetry of the Northeast Greenland continental shelf: Constraints on glacial and other
787 processes, *AGU Publ. Geochemistry Geophys. Geosystems*, 16, 267–300,
788 <https://doi.org/10.1002/2014GC005684>.Key, 2015.

789 Arndt, J. E., Jokat, W., and Dorschel, B.: The last glaciation and deglaciation of the Northeast

- 790 Greenland continental shelf revealed by hydro-acoustic data, *Quat. Sci. Rev.*, 160, 45–56, 2017.
- 791 Batchelor, C. L., Dowdeswell, J. A., and Rignot, E.: Submarine landforms reveal varying rates
792 and styles of deglaciation in North-West Greenland fjords, *Mar. Geol.*, 402, 60–80,
793 <https://doi.org/10.1016/j.margeo.2017.08.003>, 2018.
- 794 Bennike, O. and Björck, S.: Chronology of the last recession of the Greenland Ice Sheet, *J.*
795 *Quat. Sci.*, 17, 211–219, <https://doi.org/10.1002/jqs.670>, 2002.
- 796 Bennike, O. and Weidick, A.: Late Quaternary history around Nioghalvfjærdsfjorden and
797 Jøkelbugten, North-East Greenland, *Boreas*, 30, 205–227, <https://doi.org/10.1111/j.1502-3885.2001.tb01223.x>, 2001.
- 799 Bennike, O., Sørensen, M., Fredskild, B., Jacobsen, B. H., Böcher, J., Amsinck, S. L.,
800 Jeppesen, E., Andreasen, C., Christiansen, H. H., and Humlum, O.: Late Quaternary
801 Environmental and Cultural Changes in the Wollaston Forland Region, Northeast Greenland,
802 *Adv. Ecol. Res.*, 40, 45–79, [https://doi.org/10.1016/S0065-2504\(07\)00003-7](https://doi.org/10.1016/S0065-2504(07)00003-7), 2008.
- 803 Bentley, C. R.: Antarctic ice streams: a review, *Geophys. Res.*, 92(6), 8843–8858, 1987.
- 804 Biette, M., Jomelli, V., Chenet, M., Braucher, R., Rinterknecht, V., and Lane, T.: Mountain
805 glacier fluctuations during the Lateglacial and Holocene on Clavering Island (northeastern
806 Greenland) from ¹⁰Be moraine dating, *Boreas*, 49, 873–885, <https://doi.org/10.1111/bor.12460>,
807 2020.
- 808 Björck, S. and Persson, T.: Late Weichselian and Flandrian biostratigraphy and chronology from
809 hochstetter forland, northeast Greenland, *Medd. Om. Grøn. Geosci.*, 5, 1–19, 1981.
- 810 Björck, S., Wohlfarth, B., Bennike, O., Hjort, C., and Persson, T.: Revision of the early Holocene
811 lake sediment based chronology and event stratigraphy on Hochstetter Forland, NE Greenland,
812 *Boreas*, 23, 513–523, <https://doi.org/10.1111/j.1502-3885.1994.tb00619.x>, 1994.
- 813 Boulton, G. S. and Deynoux, M.: Sedimentation in glacial environments and the identification of
814 tills and tillites in ancient sedimentary sequences, *Precambrian Res.*, 15, 397–422,
815 [https://doi.org/10.1016/0301-9268\(81\)90059-0](https://doi.org/10.1016/0301-9268(81)90059-0), 1981.
- 816 Boulton, G. S., Hagdorn, M., and Hulton, N. R. J.: Streaming flow in an ice sheet through a
817 glacial cycle, *Ann. Glaciol.*, 36, 117–128, <https://doi.org/10.3189/172756403781816293>, 2003.
- 818 Briner, J. P., McKay, N. P., Axford, Y., Bennike, O., Bradley, R. S., de Vernal, A., Fisher, D.,
819 Francus, P., Fréchette, B., Gajewski, K., Jennings, A., Kaufman, D. S., Miller, G., Rouston, C.,
820 and Wagner, B.: Holocene climate change in Arctic Canada and Greenland, *Quat. Sci. Rev.*,
821 147, 340–364, <https://doi.org/10.1016/j.quascirev.2016.02.010>, 2016.
- 822 Cartigny, M. J. B., Postma, G., Berg, J. H., and Mastbergen, D. R.: A comparative study of
823 sediment waves and cyclic steps based on geometries, internal structures and numerical
824 modeling, *Mar. Geol.*, 280, 40–56, 2011.
- 825 Christiansen, J. S.: The TUNU-Programme : Euro-Arctic Marine Fishes — Diversity and
826 Adaptation, in: *Adaptation and Evolution in Marine Environments*, vol. 1, 35–50,
827 <https://doi.org/10.1007/978-3-642-27352-0>, 2012.
- 828 Clark, C. D.: Mega-scale lineations and cross-cutting ice-flow landforms, *Earth Surf. Process.*
829 *Landforms*, 18, 1–29, 1993.
- 830 Clark, C. D. and Stokes, C. R.: Palaeo-ice stream landsystem, in: *Glacial Landscapes*, edited

- 831 by: Evans, D. J. A., Edward Arnold, London, 204–227, 2003.
- 832 Clark, C. D., Tulaczyk, S. M., Stokes, C. R., and Canals, M.: A groove-ploughing theory for the
833 production of mega-scale glacial lineations, and implications for ice-stream mechanics, *J.*
834 *Glaciol.*, 49, 240–256, <https://doi.org/10.3189/172756503781830719>, 2003.
- 835 Cohen, J., Screen, J. A., Furtado, J. C., Barlow, M., Whittleston, D., Coumou, D., Francis, J.,
836 Dethloff, K., Entekhabi, D., Overland, J., and Jones, J.: Recent Arctic amplification and extreme
837 mid-latitude weather, *Nat. Publ. Gr.*, 7, 627–637, <https://doi.org/10.1038/ngeo2234>, 2014.
- 838 Cremer, H., Bennike, O., and Wagner, B.: Lake sediment evidence for the last deglaciation of
839 eastern Greenland, *Quat. Sci. Rev.*, 27, 312–319,
840 <https://doi.org/10.1016/j.quascirev.2007.09.004>, 2008.
- 841 Davies, J., Mathiasen, A. M., Kristiansen, K., Hansen, K. E., Wacker, L., Alstrup, A. K. O., Munk,
842 O. L., Pearce, C., and Seidenkrantz, M. S.: Linkages between ocean circulation and the
843 Northeast Greenland Ice Stream in the Early Holocene, *Quat. Sci. Rev.*, 286, 107530,
844 <https://doi.org/10.1016/j.quascirev.2022.107530>, 2022.
- 845 Dowdeswell, J. A., Ottesen, D., Evans, J., Cofaigh, C. Ó., and Anderson, J. B.: Submarine
846 glacial landforms and rates of ice-stream collapse, *Geology*, 36, 819–822,
847 <https://doi.org/10.1130/G24808A.1>, 2008.
- 848 Dowdeswell, J. A., Hogan, K. A., Ó Cofaigh, C., Fugelli, E. M. G., Evans, J., and Noormets, R.:
849 Late Quaternary ice flow in a West Greenland fjord and cross-shelf trough system: submarine
850 landforms from Rink Isbrae to Uummannaq shelf and slope, *Quat. Sci. Rev.*, 92, 292–309,
851 2014.
- 852 Dowdeswell, J. A., Canals, M., Jakobsson, M., Todd, B. J., Dowdeswell, E. K., and Hogan, K.
853 A.: The variety and distribution of submarine glacial landforms and implications for ice-sheet
854 reconstruction, *Geol. Soc. Mem.*, 46, 519–552, <https://doi.org/10.1144/M46.183>, 2016.
- 855 Evans, J., Dowdeswell, J. A., Grobe, H., Niessen, F., Stein, R., Hubberten, H. W., and
856 Whittington, R. J.: Late Quaternary sedimentation in Kejser Franz Joseph Fjord and the
857 continental margin of East Greenland, *Geol. Soc. Spec. Publ.*, 203, 149–179,
858 <https://doi.org/10.1144/GSL.SP.2002.203.01.09>, 2002.
- 859 Evans, J., Ó Cofaigh, C., Dowdeswell, J. A., and Wadhams, P.: Marine geophysical evidence
860 for former expansion and flow of the Greenland Ice Sheet across the north-east Greenland
861 continental shelf, *J. Quat. Sci.*, 24, 279–293, 2009.
- 862 Eyles, N., Eyles, C. H., and Niall, An. D.: Lithofacies types and vertical profile models; an
863 alternative approach to the description and environmental interpretation of glacial diamict and
864 diamictite sequences, *Sedimentology*, 30, 393–410, 1983.
- 865 Folk, R. L.: The Distinction between Grain Size and Mineral Composition in Sedimentary-Rock
866 Nomenclature, *J. Geol.*, 62, 344–359, 1954.
- 867 Folk, R. L. and Ward, W.: Brazos river bar, a study in the significance of grain size parameters.,
868 *J. Sediment. Petrol.*, 27, 34–59, 1957.
- 869 Forwick, M. and Vorren, T. O.: Deglaciation history and post-glacial mass movements in
870 Balsfjord, northern Norway, *Polar Res.*, 21(2), 259–266, 1998.
- 871 Forwick, M., Vorren, T. O., Hald, M., Korsun, S., Roh, Y., Vogt, C., and Yoo, K. C.: Spatial and
872 temporal influence of glaciers and rivers on the sedimentary environment in Sassenfjorden and

- 873 Tempelfjorden, Spitsbergen, *Geol. Soc. London, Spec. Publ.*, 344, 163–193,
874 <https://doi.org/10.1144/SP344.13>, 2010.
- 875 Funder, S., Kjeldsen, K. K., Kjær, H. K., and Ó Cofaigh, C.: The Greenland Ice Sheet During the
876 Past 300,000 Years: A Review, *Dev. Quat. Sci.*, 15, 699–713, <https://doi.org/10.1016/B978-0-444-53447-7.00050-7>, 2011.
- 878 Funder, S., Sørensen, A. H. L., Larsen, N. K., Bjørk, A. A., Briner, J. P., Olsen, J., Schomacker,
879 A., Levy, L. B., and Kjær, K. H.: Younger Dryas ice margin retreat in Greenland: new evidence
880 from southwestern Greenland, *Clim. Past*, 17, 587–601, 2021.
- 881 Geirsdóttir, Á., Hardardóttir, J., and Andrews, J. T.: Late-Holocene terrestrial glacial history of
882 Miki and I.C. Jacobsen Fjords, East Greenland, Holocene, 10, 123–134,
883 <https://doi.org/10.1191/095968300666213169>, 2000.
- 884 Håkansson, L., Graf, A., Strasky, S., Ivy-ochs, S., Kubik, P. W., Hjort, C., Shluchter, C.,
885 Geografiska, S., Series, A., Geography, P., Hakansson, L., Graf, A., Strasky, S., Ivy-ochs, S.,
886 Kubik, P. W., Hjort, C., and Schlichter, C.: Cosmogenic ¹⁰Be-Ages from the Store Koldewey
887 Island, NE Greenland, *Geogr. Ann. Ser. A Phys. Geogr.*, 89, 195–202, 2007.
- 888 Hansen, K. E., Lorenzen, J., Davies, J., Wacker, L., Pearce, C., and Seidenkrantz, M.-S.:
889 Deglacial to Mid Holocene environmental conditions on the northeastern Greenland shelf,
890 *Quaternary Sci. Rev.*, 293, 107704, 2022.
- 891 Heaton, T. J., Köhler, P., Butzin, M., Bard, E., Reimer, R. W., Austin, W. E. N., Ramsey, C. B.,
892 Grootes, P. M., Hughen, K. A., Kromer, B., Reimer, P. J., and Heaton, T. J.: Marine20 — The
893 Marine Radiocarbon Age Calibration Curve (0-55,000 CAL BP), *Radio*, 62, 779–820,
894 <https://doi.org/10.1017/RDC.2020.68>, 2020.
- 895 Heaton, T. J., Bard, E., Ramsey, C. B., Butzin, M., Hatté, C., Hughen, K. A., Köhler, P., and
896 Reimer, P. J.: A Response to Community Questions on the Marine20 Radiocarbon Age
897 Calibration Curve: Marine Reservoir Ages and The Calibration of ¹⁴C Samples from the
898 Oceans, *Radiocarbon*, 65, 247–273, <https://doi.org/10.1017/RDC.2022.66>, 2022.
- 899 Higgins, A. K.: North Greenland Glaciers Velocities and Calf Ice Production, *Polarforschung*, 60,
900 1–23, 1991.
- 901 Hill, P. R.: Changes in submarine channel morphology and strata development from repeat
902 multibeam surveys in the Fraser River delta, western Canada, in: *Sediments, Morphology and
903 Sedimentary Processes on Continental Shelves*, edited by: Li, M. Z., Sherwood, C. R., and Hill,
904 P. R., Blackwell Science, International Association of Sedimentologists, 47–70, 2012.
- 905 Hjort, C.: Glaciation in northern East Greenland during the Late Weichselian and Early
906 Flandrian, *Boreas*, 8, 281–296, <https://doi.org/10.1111/j.1502-3885.1979.tb00812.x>, 1979.
- 907 Hjort, C.: A glacial chronology for northern East Greenland, *Boreas*, 10, 259–274, 1981.
- 908 Hjort, C. and Björck, S.: A re-evaluated glacial chronology for Northern East Greenland, *Geol.
909 Föreningen i Stock. Förhandlingar*, 105, 235–243, <https://doi.org/10.1080/11035898309452590>,
910 1983.
- 911 Hogan, K. A., Dowdeswell, J. A., Noormets, R., Evans, J., and Ó Cofaigh, C.: Evidence for full-
912 glacial flow and retreat of the Late Weichselian Ice Sheet from the waters around Kong Karls
913 Land, eastern Svalbard, *Quat. Sci. Rev.*, 29, 3563–3582,
914 <https://doi.org/10.1016/j.quascirev.2010.05.026>, 2010.

- 915 Hogan, K. A., Ó Cofaigh, C., Jennings, A. E., Dowdeswell, J. A., and Hiemstra, J. F.:
916 Deglaciation of a major palaeo-ice stream in Disko Trough, West Greenland, *Quat. Sci. Rev.*,
917 147, 5–26, 2016.
- 918 Huddart, D. and Lister, H.: The Origin of Ice Marginal Terraces and Contact Ridges of East
919 Kangerdluarssuk Glacier, SW Greenland, *Geogr. Ann.*, 63 A, 31–39, 1981.
- 920 Jackson, R., Andreassen, N., Oksman, M., Andersen, T. J., Pearce, C., Seidenkrantz, M.-S., and
921 Ribeiro, S.: Marine conditions and development of the Sirius Water polynya on the North-East
922 Greenland shelf during the Younger Dryas-Holocene, *Quat. Sci. Rev.*, 291, 107647, 2022.
- 923 Jakobsson, M., Hogan, K. A., Mayer, L. A., Mix, A., Jennings, A., Stoner, J., Eriksson, B.,
924 Jerram, K., Mohammad, R., Pearce, C., Reilly, B., and Stranne, C.: The Holocene retreat
925 dynamics and stability of Petermann Glacier in northwest Greenland, *Nat. Commun.*, 9,
926 <https://doi.org/10.1038/s41467-018-04573-2>, 2018.
- 927 Jakobsson, M., Mayer, L. A., Bringensparr, C., Castro, C. F., Mohammad, R., Johnson, P.,
928 Ketter, T., Accettella, D., Amblas, D., An, L., Arndt, J. E., Canals, M., Casamor, J. L., Chauché,
929 N., Coakley, B., Danielson, S., Demarte, M., Dickson, M. L., Dorschel, B., Dowdeswell, J. A.,
930 Dreutter, S., Fremand, A. C., Gallant, D., Hall, J. K., Hehemann, L., Hodnesdal, H., Hong, J.,
931 Ivaldi, R., Kane, E., Klaucke, I., Krawczyk, D. W., Kristoffersen, Y., Kuipers, B. R., Millan, R.,
932 Masetti, G., Morlighem, M., Noormets, R., Prescott, M. M., Rebesco, M., Rignot, E., Semiletov,
933 I., Tate, A. J., Travaglini, P., Velicogna, I., Weatherall, P., Weinrebe, W., Willis, J. K., Wood, M.,
934 Zarayskaya, Y., Zhang, T., Zimmermann, M., and Zinglensen, K. B.: The International
935 Bathymetric Chart of the Arctic Ocean Version 4.0, *Sci. Data*, 7, 1–14,
936 <https://doi.org/10.1038/s41597-020-0520-9>, 2020.
- 937 Joughin, I., Fahnestock, M., MacAyeal, D., Bamber, J. L., and Gogineni, P.: Observation and
938 analysis of ice flow in the largest Greenland ice stream, *J. Geophys. Res. Atmos.*, 106, 34021–
939 34034, <https://doi.org/10.1029/2001JD900087>, 2001.
- 940 Kelly, M. A., Lowell, T. V., Hall, B. L., Schaefer, J. M., Finkel, R. C., Goehring, B. M., Alley, R.
941 B., and Denton, G. H.: A ^{10}Be chronology of lateglacial and Holocene mountain glaciation in the
942 Scoresby Sund region, east Greenland: implications for seasonality during lateglacial time,
943 *Quat. Sci. Rev.*, 27, 2273–2282, 2008.
- 944 Kempf, P., Forwick, M., Laberg, J. S., and Vorren, T. O.: Late Weichselian and Holocene
945 sedimentary palaeoenvironment and glacial activity in the high-arctic van Keulenfjorden,
946 Spitsbergen, *The Holocene*, 23 (11), 1607–1618, <https://doi.org/10.1177/0959683613499055>,
947 2013.
- 948 Khan, S. A., Kjær, K. H., Bevis, M., Bamber, J. L., Wahr, J., Kjeldsen, K. K., Bjørk, A. A.,
949 Korsgaard, N. J., Stearns, L. A., Van Den Broeke, M. R., Liu, L., Larsen, N. K., and Muresan, I.
950 S.: Sustained mass loss of the northeast Greenland ice sheet triggered by regional warming,
951 *Nat. Clim. Chang.*, 4, 292–299, <https://doi.org/10.1038/nclimate2161>, 2014.
- 952 King, E. C., Hindmarsh, R. C. A., and Stokes, C. R.: Formation of mega-scale glacial lineations
953 observed beneath a West Antarctic ice stream, *Nat. Geosci.*, 2, 585–588,
954 <https://doi.org/10.1038/ngeo581>, 2009.
- 955 King, M. D., Howat, I. M., Candela, S. G., Noh, M. J., Jeong, S., Noël, B. P. Y., van den Broeke,
956 M. R., Wouters, B., and Negrete, A.: Dynamic ice loss from the Greenland Ice Sheet driven by
957 sustained glacier retreat, *Commun. Earth Environ.*, 1, 1–7, <https://doi.org/10.1038/s43247-020-0001-2>,
958 2020.

- 959 Klages, J. P., Kuhn, G., Hillenbrand, C.-D., Graham, A. G. C., Smith, J. A., Larter, R. D., and
 960 Gohl, K.: First geomorphological record and glacial history of an inter-ice stream ridge on the
 961 West Antarctic continental shelf, *Quat. Sci. Rev.*, 61, 47–61, 2013.
- 962 Klages, J. P., Kuhn, G., Graham, A. G. C., Hillenbrand, C.-D., Smith, J. A., Nitsche, F. O.,
 963 Larter, R. D., and Gohl, K.: Palaeo-ice stream pathways and retreat style in the easternmost
 964 Amundsen Sea Embayment, West Antarctica, revealed by combined multibeam bathymetric
 965 and seismic data, *Geomorphology*, 245, 207–222, 2015.
- 966 Klug, M., Schmidt, S., Melles, M., Wagner, B., Bennike, O., and Heiri, O.: Lake sediments from
 967 Store Koldewey, Northeast Greenland, as archive of Late Pleistocene and Holocene climatic
 968 and environmental changes, *Boreas*, 38, 59–71, <https://doi.org/10.1111/j.1502-3885.2008.00038.x>, 2009a.
- 970 Klug, M., Bennike, O., and Wagner, B.: Repeated short-term bioproductivity changes in a
 971 coastal lake on Store Koldewey, northeast Greenland: An indicator of varying sea-ice
 972 coverage?, *Holocene*, 19, 653–663, <https://doi.org/10.1177/0959683609104040>, 2009b.
- 973 Klug, M., Bennike, O., and Wagner, B.: Late Pleistocene to early Holocene environmental
 974 changes on Store Koldewey, coastal north-east Greenland, *Polar Res.*, 35,
 975 <https://doi.org/10.3402/polar.v35.21912>, 2016.
- 976 Kobashi, T., Menviel, L., Jeltsch-Thömmes, A., Vinther, B. M., Box, J. E., Muscheler, R.,
 977 Nakaegawa, T., Pfister, P. L., Döring, M., Leuenberger, M., Wanner, H., and Ohmura, A.:
 978 Volcanic influence on centennial to millennial Holocene Greenland temperature change, *Sci.*
 979 *Rep.*, 7, 1–10, <https://doi.org/10.1038/s41598-017-01451-7>, 2017.
- 980 Kolling, H. M., Stein, R., Fahl, K., Perner, K., and Moros, M.: Short-term variability in late
 981 Holocene sea ice cover on the East Greenland Shelf and its driving mechanisms, *Palaeogeogr.*
 982 *Palaeoclimatol. Palaeoecol.*, 485, 336–350, <https://doi.org/10.1016/j.palaeo.2017.06.024>, 2017.
- 983 Krieger, L., Floricioiu, D., and Neckel, N.: Drainage basin delineation for outlet glaciers of
 984 Northeast Greenland based on Sentinel-1 ice velocities and TanDEM-X elevations, *Remote*
 985 *Sens. Environ.*, 237, 111483, <https://doi.org/10.1016/j.rse.2019.111483>, 2020.
- 986 Laberg, J. S., Forwick, M., and Husum, K.: New geophysical evidence for a revised maximum
 987 position of part of the NE sector of the Greenland ice sheet during the last glacial maximum,
 988 *Arktos*, 3, <https://doi.org/10.1007/s41063-017-0029-4>, 2017.
- 989 Lambeck, K., Rouby, H., Purcell, A., Sun, Y., and Sambridge, M.: Sea level and global ice
 990 volumes from the Last Glacial Maximum to the Holocene, *Proc. Natl. Acad. Sci.*, 111, 15296–
 991 15303, <https://doi.org/10.1073/pnas.1411762111>, 2014.
- 992 Landvik, J. Y.: The last glaciation of Germania Land and adjacent areas, northeast Greenland,
 993 *J. Quat. Sci.*, 9, 81–92, <https://doi.org/10.1002/jqs.3390090108>, 1994.
- 994 Lane, T. P., Roberts, D. H., Ó Cofaigh, C., Vieli, A., and Moreton, S. G.: The glacial history of
 995 the southern Svartehuk Halvø, West Greenland, *Arktos*, 1, 1–28,
 996 <https://doi.org/10.1007/s41063-015-0017-5>, 2015.
- 997 Larsen, N. K., Funder, S., Linge, H., Möller, P., Schomacker, A., Fabel, D., Xu, S., and Kjær, K.
 998 H.: A Younger Dryas re-advance of local glaciers in north Greenland, *Quat. Sci. Rev.*, 147, 47–
 999 58, <https://doi.org/10.1016/j.quascirev.2015.10.036>, 2016.
- 1000 Larsen, N. K., Levy, L. B., Carlson, A. E., Buizert, C., Olsen, J., Strunk, A., Bjørk, A. A., and
 1001 Skov, D. S.: Instability of the Northeast Greenland Ice Stream over the last 45,000 years, *Nat.*

- 1002 Commun., 9, 3–10, <https://doi.org/10.1038/s41467-018-04312-7>, 2018.
- 1003 Larsen, N. K., Søndergaard, A. S., Levy, L. B., Olsen, J., Strunk, A., Bjørk, A. A., and Skov, D.:
 1004 Contrasting modes of deglaciation between fjords and inter-fjord areas in eastern North
 1005 Greenland, *Boreas*, 49, 905–919, <https://doi.org/10.1111/bor.12475>, 2020.
- 1006 Larsen, N. K., Søndergaard, A. S., Levy, L. B., Strunk, A., Skov, D. S., Bjørk, A., Khan, S. A.,
 1007 and Olsen, J.: Late glacial and Holocene glaciation history of North and Northeast Greenland,
 1008 *Arctic, Antarct. Alp. Res.*, 54, 294–313, <https://doi.org/10.1080/15230430.2022.2094607>, 2022.
- 1009 Lecavalier, B. S., Milne, G. A., Simpson, M. J. R., Wake, L., Huybrechts, P., Tarasov, L.,
 1010 Kjeldsen, K. K., Funder, S., Long, A. J., Woodroffe, S., Dyke, A. S., and Larsen, N. K.: A model
 1011 of Greenland Ice Sheet deglaciation constrained by observations of relative sea level and ice
 1012 extent, *Quat. Sci. Rev.*, 102, 54–84, 2014.
- 1013 Levy, L. B., Kelly, M. A., Lowell, T. V., Hall, B. L., Howley, J. A., and Smith, C. A.: Coeval
 1014 fluctuations of the Greenland ice sheet and a local glacier, central East Greenland, during late
 1015 glacial and early Holocene time, *Geophys. Res. Lett.*, 43, 1623–1631, 2016.
- 1016 Lyså, A. and Vorren, T. O.: Seismic facies and architecture of ice-contact submarine fans in
 1017 high-relief fjords, Troms, Northern Norway, *Boreas*, 26, 309–328, 1997.
- 1018 Mouginit, J., Rignot, E., Scheuchl, B., Fenty, I., Khazendar, A., Morlighem, M., Buzzi, A., and
 1019 Paden, J.: Fast retreat of Zachariae Isstrom, Northeast Greenland, *Science (80-.)*, 350, 1357–
 1020 1361, 2015.
- 1021 Mouginit, J., Bjørk, A. A., Millan, R., Scheuchl, B., and Rignot, E.: Insights on the Surge
 1022 Behavior of Storstrømmen and L. Bistrup Bræ, Northeast Greenland, Over the Last Century,
 1023 *Geophys. Res. Lett.*, 45, 11,197-11,205, <https://doi.org/10.1029/2018GL079052>, 2018.
- 1024 Newton, A. M. W., Knutz, P. C., Huuse, M., Gannon, P., Brocklehurst, S. H., Clausen, O. R.,
 1025 and Gong, Y.: Ice stream reorganization and glacial retreat on the northwest Greenland shelf,
 1026 *Geophys. Res. Lett.*, 44, 7826–7835, <https://doi.org/10.1002/2017GL073690>, 2017.
- 1027 Ó Cofaigh, C.: Flow Dynamics and till genesis associated with a marin-based Antarctic palaeo-
 1028 ice stream, *Quat. Sci. Rev.*, 24, 709–740, 2005.
- 1029 Ó Cofaigh, C., Dowdeswell, J. A., and Grobe, H.: Holocene glacimarine sedimentation, inner
 1030 Scoresby Sund, East Greenland: The influence of fast-flowing ice-sheet outlet glaciers, *Mar.*
 1031 *Geol.*, 175, 103–129, [https://doi.org/10.1016/S0025-3227\(01\)00117-7](https://doi.org/10.1016/S0025-3227(01)00117-7), 2001.
- 1032 Ó Cofaigh, C., Dowdeswell, J. A., Jennings, A. E., Hogan, K. A., Kilfeather, A., Hiemstra, J. F.,
 1033 Noormets, R., Evans, J., McCarthy, D. J., Andrews, J. T., Lloyd, J. M., and Moros, M.: An
 1034 extensive and dynamic ice sheet on the west greenland shelf during the last glacial cycle,
 1035 *Geology*, 41, 219–222, <https://doi.org/10.1130/G33759.1>, 2013.
- 1036 Olsen, I. L., Forwick, M., Laberg, J. S., and Rydningen, T. A.: Last Glacial ice-sheet dynamics
 1037 offshore NE Greenland – a case study from Store Koldewey Trough, *The Cryosphere*
 1038 *Discussions*, 2020.
- 1039 Ottesen, D., Dowdeswell, J. A., and Rise, L.: Submarine landforms and the reconstruction of
 1040 fast-flowing ice streams within a large Quaternary ice sheet: The 2500-km-long Norwegian-
 1041 Svalbard margin (57°-80°N), *Bull. Geol. Soc. Am.*, 117, 1033–1050,
 1042 <https://doi.org/10.1130/B25577.1>, 2005.
- 1043 Ottesen, D., Dowdeswell, J. A., Benn, D. I., Kristensen, L., Christiansen, H. H., Christensen, O.,

- 1044 Hansen, L., Lebesbye, E., Forwick, M., and Vorren, T. O.: Submarine landforms characteristic of
1045 glacier surges in two spitsbergen fjords, *Quat. Sci. Rev.*, 27, 1583–1599, 2008.
- 1046 Pados-Dibattista, T., Pearce, C., Detlef, H., Bendtsen, J., and Seidenkrantz, M. S.: Holocene
1047 palaeoceanography of the Northeast Greenland shelf, *Clim. Past*, 18, 103–127,
1048 <https://doi.org/10.5194/cp-18-103-2022>, 2022.
- 1049 Pedersen, J. B. T., Kroon, A., and Jakobsen, B. H.: Holocene sea-level reconstruction in the
1050 Young Sound region, Northeast Greenland, *J. Quat. Sci.*, 26(2), 219–226, 2011.
- 1051 Rahmstorf, S., Box, J. E., Feulner, G., Mann, M. E., Robinson, A., Rutherford, S., and
1052 Schaffernicht, E. J.: Exceptional twentieth-century slowdown in Atlantic Ocean overturning
1053 circulation, *Nat. Clim. Chang.*, 5, 475–480, <https://doi.org/10.1038/nclimate2554>, 2015.
- 1054 Rasmussen, T. L., Pearce, C., Andresen, K. J., Nielsen, T., and Seidenkrantz, M.-S.: Northeast
1055 Greenland: ice-free shelf edge at 79.4°N around the Last Glacial Maximum 25.5–17.5 ka,
1056 *Boreas*, 51, 759–775, 2022.
- 1057 Reeh, N., Bøggild, C. E., and Oerter, H.: Surge of Storstrømmen, a large outlet glacier from the
1058 Inland Ice of North-East Greenland, *Rapp. Grønlands Geol. Unders.*, 162, 201–209, 1994.
- 1059 Reilly, B. T., Stoner, J. S., Mix, A. C., Walczak, M. H., Jennings, A., Jakobsson, M., Dyke, L.,
1060 Glueder, A., Nicholls, K., Hogan, K. A., Mayer, L. A., Hatfield, Robert, G., Albert, S., Marcott, S.,
1061 Fallon, S., and Cheseby, M.: Holocene break-up and reestablishment of the Petermann Ice
1062 Tongue, Northwest Greenland, *Quat. Sci. Rev.*, 218, 322–342, 2019.
- 1063 Reimer, P. J., Austin, W. E. N., Bard, E., Bayliss, A., Blackwell, P. G., Bronk Ramsey, C.,
1064 Butzin, M., Cheng, H., Edwards, R. L., Friedrich, M., Grootes, P. M., Guilderson, T. P., Hajdas,
1065 I., Heaton, T. J., Hogg, A. G., Hughen, K. A., Kromer, B., Manning, S. W., Muscheler, R.,
1066 Palmer, J. G., Pearson, C., Van Der Plicht, J., Reimer, R. W., Richards, D. A., Scott, E. M.,
1067 Southon, J. R., Turney, C. S. M., Wacker, L., Adolphi, F., Büntgen, U., Capano, M., Fahrni, S.
1068 M., Fogtmann-Schulz, A., Friedrich, R., Köhler, P., Kudsk, S., Miyake, F., Olsen, J., Reinig, F.,
1069 Sakamoto, M., Sookdeo, A., and Talamo, S.: The IntCal20 Northern Hemisphere Radiocarbon
1070 Age Calibration Curve (0-55 cal kBP), *Radiocarbon*, 62, 725–757,
1071 <https://doi.org/10.1017/RDC.2020.41>, 2020.
- 1072 Rignot, E., Bjork, A., Chauche, N., and Klauke, I.: Storstrømmen and L. Bistrup Bræ, North
1073 Greenland, Protected From Warm Atlantic Ocean Waters, *Geophys. Res. Lett.*, 49,
1074 <https://doi.org/10.1029/2021GL097320>, 2022.
- 1075 Rydningen, T. A., Vorren, T. O., Laberg, J. S., and Kolstad, V.: The marine-based NW
1076 Fennoscandian ice sheet: Glacial and deglacial dynamics as reconstructed from submarine
1077 landforms, *Quat. Sci. Rev.*, 68, 126–141, <https://doi.org/10.1016/j.quascirev.2013.02.013>, 2013.
- 1078 Sættem, J.: Glaciotectonic forms and structures on the Norwegian continental shelf:
1079 observations, processes and implications, *Nor. Geol. Tidsskr.*, 70, 81–94, 1990.
- 1080 Schaffer, J., von Appen, W.-J., Dodd, P. A., Hofstede, C., Mayer, C., de Steur, L., and Kanzow,
1081 T.: Warm water pathways toward Nioghalvfjærdsfjorden Glacier, Northeast Greenland, *J.*
1082 *Geophys. Res. Ocean.*, 122, 4004–4020, <https://doi.org/10.1002/2016JC012462>.Received,
1083 2017.
- 1084 Schmidt, S., Wagner, B., Heiri, O., Klug, M., Bennike, O., and Melles, M.: Chironomids as
1085 indicators of the Holocene climatic and environmental history of two lakes in Northeast
1086 Greenland, *Boreas*, 40, 116–130, <https://doi.org/10.1111/j.1502-3885.2010.00173.x>, 2011.

- 1087 Schoof, C. G. and Clarke, G. K. C.: A model for spiral flows in basal ice and the formation of
1088 subglacial flutes based on a Reiner-Rivlin rheology for glacial ice, *J. Geophys. Res. Solid Earth*,
1089 113, 1–12, <https://doi.org/10.1029/2007JB004957>, 2008.
- 1090 Shaw, J., Pugin, A., and Young, R. R.: A meltwater origin for Antarctic shelf bedforms with
1091 special attention to megalineations, *Geomorphology*, 102, 364–375,
1092 <https://doi.org/10.1016/j.geomorph.2008.04.005>, 2008.
- 1093 Shreve, R. L.: Esker characteristics in terms of glacier physics, Katahdin esker system, Maine.,
1094 *Geol. Soc. Am. Bull.*, 96, 639–646, [https://doi.org/10.1130/0016-7606\(1985\)96<639:ECITOG>2.0.CO;2](https://doi.org/10.1130/0016-7606(1985)96<639:ECITOG>2.0.CO;2), 1985.
- 1096 Skov, D. S., Andersen, J. L., Olsen, J., Jacobsen, B. H., Knudsen, M. F., Jansen, J. D., Larsen,
1097 N. K., and Egholm, D. L.: Constraints from cosmogenic nuclides on the glaciation and erosion
1098 history of Dove Bugt, northeast Greenland, *GSA Bull.*, 1–13, 2020.
- 1099 Slabon, P., Dorschel, B., Jokat, W., Myklebust, R., Hebbeln, D., and Gebhardt, C.: Greenland
1100 ice sheet retreat history in the northeast Baffin Bay based on high-resolution bathymetry, *Quat.*
1101 *Sci. Rev.*, 154, 182–198, <https://doi.org/10.1016/j.quascirev.2016.10.022>, 2016.
- 1102 Smith, L. M. and Andrews, J. T.: Sediment characteristics in iceberg dominated fjords,
1103 Kangerlussuaq region, East Greenland, *Sediment. Geol.*, 130, 11–25,
1104 [https://doi.org/10.1016/S0037-0738\(99\)00088-3](https://doi.org/10.1016/S0037-0738(99)00088-3), 2000.
- 1105 Stacey, C. D. and Hill, P. R.: Cyclic steps on a glacial delta, Howe Sound, British Columbia,
1106 in: *Atlas of Submarine Glacial Landforms: Modern, Quaternary and Ancient*, edited by:
1107 Dowdeswell, J. A., Canals, M., Jakobsson, M., Todd, B. J., Dowdeswell, E. K. & Hogan, K. A.,
1108 Geological Society of London, 93–94, 2016.
- 1109 Stocker, T. F., Qin, D., Plattner, G.-K., Tignor, M. M. B., Allen, S. K., Boschung, J., Nauels, A.,
1110 Xia, Y., Bex, V., and Midgley, P. M.: *Climate Change 2013: The Physical Science Basis.*
1111 Contribution of Working Group I to the Fifth Assessment Report of the Intergovernmental Panel
1112 on Climate Change, Cambridge, 2013.
- 1113 Stokes, C. R. and Clark, C. D.: Geomorphological criteria for identifying Pleistocene ice
1114 streams, *Ann. Glaciol.*, 28, 67–74, <https://doi.org/10.3189/172756499781821625>, 1999.
- 1115 Stokes, C. R. and Clark, C. D.: Palaeo-ice streams, *Quat. Sci. Rev.*, 20, 1437–1457, 2001.
- 1116 Storrar, R. D., Stokes, C. R., and Evans, D. J. A.: Morphometry and pattern of a large sample
1117 (>20,000) of Canadian eskers and implications for subglacial drainage beneath ice sheets,
1118 *Quat. Sci. Rev.*, 105, 1–25, <https://doi.org/10.1016/j.quascirev.2014.09.013>, 2014.
- 1119 Syring, N., Lloyd, J. M., Stein, R., Fahl, K., Roberts, D. H., Callard, L., and O’Cofaigh, C.:
1120 Holocene interactions between glacier retreat, sea ice formation, and Atlantic water advection at
1121 the inner Northeast Greenland continental shelf, *Paleoceanogr. Paleoclimatology*, 35, 2020.
- 1122 Wagner, B., Bennike, O., Bos, J. A. A., Cremer, H., Lotter, A. F., and Melles, M.: A
1123 multidisciplinary study of Holocene sediment records from Hjort Sø on Store Koldewey,
1124 Northeast Greenland, *J. Paleolimnol.*, 39, 381–398, <https://doi.org/10.1007/s10933-007-9120-3>,
1125 2008.
- 1126 Weber, M. E., Niessen, F., Kuhn, G., and Wiedicke, M.: Calibration and application of marine
1127 sedimentary physical properties using a multi-sensor core logger, *Mar. Geol.*, 136, 151–172,
1128 1997.

- 1129 Weidick, A., Andreasen, C., Oerter, H., and Reeh, N.: Neoglacial glacier changes around
1130 Storstrommen, north-east Greenland, *Polarforschung*, 64, 95–108, 1994.
- 1131 Wilson, N. J. and Straneo, F.: Water exchange between the continental shelf and the cavity
1132 beneath Nioghalvfjærdsbræ (79 North Glacier), *Geophys. Res. Lett.*, 42, 7648–7654,
1133 <https://doi.org/10.1002/2015GL064944>, 2015.
- 1134 Winkelmann, D., Jokat, W., Jensen, L., and Schenke, H. W.: Submarine end moraines on the
1135 continental shelf off NE Greenland - Implications for Lateglacial dynamics, *Quat. Sci. Rev.*, 29,
1136 1069–1077, <https://doi.org/10.1016/j.quascirev.2010.02.002>, 2010.
- 1137